Supporting Information for:

Methane Storage in Paddlewheel-Based Porous Coordination Cages

Casey A. Rowland,[†] Gregory R. Lorzing,[†,§,‡] Eric J. Gosselin,[†,§,‡] Benjamin A. Trump,[£,‡] Glenn P. A. Yap,[†] Craig M. Brown,[¶,£] Eric D. Bloch*[,†,§]

[†]Department of Chemistry and Biochemistry, and [¶]Department of Chemical and Biomolecular Engineering, University of Delaware, Newark, Delaware 19716 United States

[§]Center for Neutron Science, Department of Chemical and Biomolecular Engineering, University of Delaware, Newark, Delaware 19716, United States

[£]Center for Neutron Research, National Institute of Standards and Technology, Gaithersburg, Maryland 20899, United States

[‡]These authors contributed equally.

J. Am. Chem. Soc.

List of Contents

Experimental Section

General Considerations. All reagents were obtained from commercial vendors and used without purification, excluding solvents. Methanol was obtained from a solvent drying system and stored in a glove box under 3Å. Thermogravimetric analyses (TGA) were carried out from 50°C to 600°C at a 2°C min^{-1} heating rate with a TA Q5000 SA under a nitrogen environment. Low-pressure adsorption measurements were obtained on a Micromeritics 3Flex. High-pressure isotherms were measured with a PCTPro-2000 Volumetric Adsorption Analyzer Infrared spectroscopy was performed on a material using a Bruker Tensor 27 instrument. Chromium and molybdenum samples were run in degassed paraffin oil. The paraffin oil was run as a background to be later subtracted from the spectra.

Note: Certain commercial equipment, instruments, or materials are identified in this document. Such identification does not imply recommendation or endorsement by the National Institute of Standards and Technology nor does it imply that the products identified are necessarily the best available for the purpose.

Synthesis of H_2cdc.[1,2] The ligand was synthesized by modified literature procedures. NaCl (50 g) was dried overnight in a 130 °C oven and added to a three-neck round bottom flask. The flask was then fitted with an addition funnel filled with H_2SO_4 solution (50 mL, 18 M). In a second three-neck flask carbazole (5 g, 29.9 mmol), trichloroacetonitrile (7.2 mL, 71.8 mmol), and chlorobenzene (120 mL) were stirred at room temperature for two hours under a nitrogen atmosphere. Anhydrous $AlCl_3$ (9.6 g, 72 mmol) was then added to the carbazole mixture and the flask was fitted with a condenser which was connected to nitrogen and a water bubbler. The reaction flask was then connected to the flask containing the NaCl via a tygon cannula. H_2SO_4 was added dropwise over the NaCl for 20 mins to generate dry HCl (g). The HCl (g) flowed through the reaction for 2 h. The tygon cannula was then removed and the reaction flask was heated to 60 °C for 30 mins, 100 °C for 2 h and then refluxed for 4 h under nitrogen. After cooling to room temperature, the reaction mixture was treated with HCl solution (25 mL, 12 M). The reaction was then refluxed for an additional 2 h under nitrogen. After cooling to room temperature, the reaction mixture was concentrated under reduced pressure. The solid residue was treated with aqueous KOH solution (150 mL, 2M) and refluxed for 2 h. Activated carbon (5 g) was then added to the reaction mixture which continued refluxing for an additional 2 h. After cooling to room temperature, the reaction mixture was filtered and the filtrate was acidified to pH = 2 with 12 M HCl to yield a pale-yellow precipitate. The precipitate was collected, washed with water and dried at 130 °C to yield white solid.

Synthesis of 9,9'-(1,4-phenylene)bis-cdc.[3] The ligand was synthesized by modified literature procedures. Dimethyl 9H-carbaozle-3,6-dicarboxylate (1 g, 3.53 mmol), K_2CO_3 (2 g, 14.471 mmol), 1,4-diiodobenzene (500 mg, 1.516 mmol), N,N'-dimethylethylenediamine (100 µL) and 1,4-dioxane (20 mL) were added to a one port schlenk flask. The flask was freeze pump thawed for three cycles to remove O_2 and then pumped into a glovebox to add CuI (50 mg, 0.263 mmol). The flask was then sealed and removed from the glovebox and set to heat at 120 °C for three days. After cooling to room temperature, the reaction mix was washed with ethyl acetate and acetone (3x's each) and the precipitated solids were collected via vacuum filtration. The solids were added to a 250 mL round bottom flask containing a 1:1:2 mix of MeOH:THF:2 M NaOH (aq) (25mL:25mL:50mL). The reaction mix was refluxed at 75 °C until the solution became clear. The reaction mix was then filtered and washed with DI H_2O. The filtrate was collected and organics

removed under reduced pressure. The aqueous solution was then acidified with 3 M HCl (aq) to pH = 1. The precipitated solids were collected via vacuum filtration and washed with DI H_2O.

Synthesis of $Cr_2(OAc)_4$.[4] Cr powder (3 g, 57.69 mmol) and HBr (2 mL) were heated to reflux in a solution of acetic anhydride (20 mL) and acetic acid (80 mL) using a dry round bottom flask (250 mL) with a reflux condenser attached for 48 h under nitrogen. Upon cooling, solid crashed out of solution as a brick red powder. The powder was isolated by vacuum filtration using a frit and dried before being stored under N_2.

Synthesis of $Cr_{12}(cdc)_{12}$. $Cr_2(OAc)_4$ (100 mg, 0.292 mmol) and H_2cdc (75 mg, 0.294 mmol) were dissolved in 10 mL of a 4:1 mixture of DMF/MeOH in a 20 mL scintillation vial. The vial was heated at 70 C for 12 h after which octahedral red crystals formed. The solvent was decanted and fresh MeOH was added. The crystals were soaked for 3 days, exchanging the solvent every 24 h. The resulting powder was dried over a frit and stored under nitrogen.

Synthesis of $Cu_{12}(cdc)_{12}$. $Cu(NO_3)_2 \cdot 2.5\ H_2O$ (46.5 mg, 0.2 mmol) and H_2cdc (50 mg, 0.2 mmol) were dissolved in 15 mL of a 1:1 mixture of DMF/EtOH in a 20 mL scintillation vial. The vial was then heated at 95 °C for 12 h after which octahedral blue/green crystals formed. The solvent was decanted and the crystals collected. The crystals were then brought into a nitrogen glovebox and the solvent exchanged by soaking the crystals in fresh MeOH for 2-3 days, exchanging the solvent every 8 h. The resulting powder was dried through active vacuum in the glove box and stored under nitrogen.

Synthesis of $Mo_{12}(cdc)_{12}$. $Mo_2(OAc)_4$ (67 mg, 0.16 mmol) was dissolved in 8 mL DEF in a 20 mL scintillation vial, H_2cdc (80 mg, 0.32 mmol) was dissolved in 7 mL DEF in a 7 mL scintillation vial. These stock solutions were heated overnight at 100 °C. The solutions were cooled to room temperature, combined in a 20 mL scintillation vial and heated to 100 °C for 12 h. The solvent was decanted and the crystals collected. The crystals were solvent exchanged by soaking in fresh MeOH for 2-3 days, exchanging the solvent every 8 h. The resulting powder was dried through active vacuum in the glove box and stored under nitrogen.

Synthesis of PCN-81.[3] The material was synthesized by a modified literature procedure. 9,9'-(1,4-phenylene)bis-cdc (50 mg, 0.085 mmol) was dissolved in 18 mL of a 1:2 mixture of DMSO/DMA. After the ligand was fully dissolved $Cu(NO_3)_2 \cdot 2.5\ H_2O$ (145 mg, 0.623 mmol) and the reaction mixture was heated to 85 °C for 3 days. The solvent was decanted and the crystals collected. The crystals were solvent exchanged with DMF for three days, exchanging the solvent every 8 hours followed by a similar methanol exchange. The sample was activated by heating to 100 °C under dynamic vacuum for two days.

X-ray structural analysis for **$Cu_{12}(cdc)_{12}$**, **$Cr_{12}(cdc)_{12}$**, and **$Mo_{12}(cdc)_{12}$**: Crystals were mounted using viscous oil onto a plastic mesh and cooled to the data collection temperature. Data were collected on a Bruker-AXS APEX II DUO CCD diffractometer with graphite-monochromated Mo-Kα radiation (λ=0.71073 Å) for **$Cu_{12}(cdc)_{12}$** and **$Cr_{12}(cdc)_{12}$**, and with Cu-Kα radiation (λ = 1.54178 Å) focused with Goebel mirrors for **$Mo_{12}(cdc)_{12}$**. Unit cell parameters were obtained from 36 data frames, 0.5º ω, from three different sections of the Ewald sphere. The systematic absences

in the diffraction data are uniquely consistent with $P2_1/n$ for **$Cu_{12}(cdc)_{12}$** and **$Mo_{12}(cdc)_{12}$**. No symmetry higher than triclinic was observed for **$Cr_{12}(cdc)_{12}$**. Refinement in the centrosymmetric space group option yielded chemically reasonable and computationally stable results of refinement. The data were treated with multi-scan absorption corrections.[5] Structures were solved using intrinsic phasing methods[6] and refined with full-matrix, least-squares procedures on F^2.[7] The three compound molecules were each located on inversion centers.

The disordered contents of highly porous metal-organic framework (MOF) and molecular cage complexes result in diffraction data that are limited in coverage and resolution. As a result, it is common to have multiple restraints and constraints, incompletely identified moieties, and high residuals in the structural model.[8] In the case of **$Mo_{12}(cdc)_{12}$**, replacing the atomic identities of the metals from Zr to Ru did not significantly change the ~2 eÅ^{-3} residual density on the metal atoms that is flagged as a level A checkCIF alert. No other transition metals were used in the synthesis other than Mo. Platon suggests no alternative unit cells or pseudomerohedral twinning matrices.[9]

Although the crystals were grown from DMF, apparent water molecules or oxygen atoms in these structures were assigned however we cannot preclude disorder masking proper assignment of solvent atoms. Thus, the apparent water molecules in **$Cu_{12}(cdc)_{12}$** appear not to be H-bonded giving rise to level B alerts. Other similar level B alerts occur in **$Cr_{12}(cdc)_{12}$** and **$Mo_{12}(cdc)_{12}$** ultimately caused by the less than satisfactory crystal quality typical of these metal organic polyhedral complexes. The formulas reported herein reflect only the atoms that were discretely modeled. Presumably disordered solvent molecules were treated as diffused contributions.[10] Non-hydrogen atoms were refined with anisotropic displacement parameters. Hydrogen atoms were treated as idealized contributions with geometrically calculated positions and with U_{iso} equal to 1.2 U_{eq} (1.5 U_{eq} for methyl) of the attached atom. Atomic scattering factors are contained in the SHELXTL program library.[6]

Neutron Powder Diffraction Experimental

Neutron powder diffraction measurements were performed on ≈ 0.3 g PCN-81 at the National Institute of Standards and Technology Center for Neutron Research (NCNR). Data was collected using a Ge(311) monochromator with an in-pile 60’ collimator, corresponding to a neutron wavelength of 2.0775 Å, using the high-resolution neutron powder diffractometer, BT-1. Samples were placed into vanadium sample cans, inside a helium-purged glovebox, and sealed with an indium o-ring onto a copper heating block containing a valved outlet for gas loading. The assembly was then mounted onto a bottom-loading closed cycle refrigerator (CCR) and connected to a gas manifold of known volume.

Diffraction measurements were conducted at base temperature for the CCR ($T \approx 7$ K), with heating up to 120 K before each stoichiometric methane dose. Additionally, adsorption was verified barometrically before cooling to base temperature to avoid condensation of the vapor phase.

Inelastic Neutron Spectroscopy (INS) was conducted on the BT-4 Filter Analyzer Neutron Spectrometer (FANS)[11], at the NCNR, using a pyrolytic graphite monochromator with 20’-40’ collimation for low energy and a copper monochromator with 60’-40’ collimation for higher energy. Measurements and gas loading were conducted using the above methods for neutron diffraction. In addition, ≈ 90 torr of helium gas was added to ensure temperature stability.

Structure Solution

Neutron powder diffraction data was analyzed using Topas Academic.[12] Initial Pawley refinements confirmed phase purity,[13] using space group (*Pa*-3) and unit cell from previously reported PCN-81.[3] Structures were then solved using the global optimization method of simulated annealing (SA) in real space,[14] followed by systematic Rietveld refinements.[15]

More specifically, for SA refinements on the bare PCN-81, the position and rotation of a rigid body 9,9′-(1,4-phenylene)bis-cdc linker was allowed to refine according to chemical restraints, including slight deviations in bond angles in the linker. Once a suitable solution was found, further Rietveld refinements were conducted to ensure the solution was at a global minimum. The bare structure was then used to determine appropriate peak shape parameters (particle size and axial divergence) for the remaining refinements. The final solution also indicated that the central benzene in the linker has two degenerate configurations, neither of which are sterically hindered.

The resulting bare structure contains Cu-paddlewheels which appear distorted, relative to the carbazole linkers. Refinements which did not allow for this structural flexibility resulted not only in statistically worse fits (≈10 % difference), but also resulted in Cu-O bond distances that were chemically unreasonable. Though the paddlewheels appear distorted, O-Cu-O angles, Cu-Cu distances, and Cu-O distances are all in agreement with previously reported Cu-paddlewheel structures.[16] This observation clarifies that relative to the Cu atoms, the paddlewheel is not distorted, and this structural flexibility is allowed due to Cu-O ionic bonding.

Once the bare structure was finalized using the previously reported space group of *Pa*-3,[3] checkCIF reported that additional symmetry was observed using PLATON.[9] Due to this observation, ADDSYM was run in PLATON, which suggested additional *C*-centering. However, this additional symmetry was not present when using ADDSYM-EXACT. PCN-82 crystallizes in *Fm*-3*m*.[3] These inconsistencies led to Pawley refinement tests, where Hamilton R-ratio tests[17] confirmed, with 99% certainty, that *Pa*-3 is preferred over *Fm*-3*m*. These refinement tests were conducted using only $Q < 1$ Å^{-1}, with higher angles not being as consistent, due to the large unit cell and changes in symmetry, although refinements were consistently ~15% better using space group *Pa*-3. Due to these differences, it is likely that space group *Fm*-3*m* approximates PCN-81 well, though it denies the structural flexibility that appears to be present.

Initial methane positions were also determined using SA refinements, followed by systematic Rietveld refinements, determining whether refinements were sensitive to methane orientation. Namely, if each methane was orientationally disordered over a sphere, rotationally disordered over two positions, or had a unique solution. This led to four types of methane positions/orientations; a central methane, a paddlewheel methane disordered over two orientations, inner corner methane disordered over two orientations, and methane in the windows of the pores with a unique orientation. Once these orientations were confirmed, occupancies and thermal parameters were refined, with occupancies that refined within error of unity being fixed.

Of these four positions, two have been previously observed. The paddlewheel site is analogous to the metal site observed for methane adsorption in HKUST-1,[16] and both are rotationally disordered. For this structure however, the methane appears off centered, and is shifted towards the most sterically accessible paddlewheel oxygen. This is consistent with methane preferring to adsorb with oxygen over an open metal site. This site also appears split between opposite sides of the paddlewheel, with a second site closer to the inner corner of the pore, again suggesting that methane has stronger interactions with the pore walls than the open metal site.

The methane sites in the pore walls are also analogous to methane adsorption in HKUST-1, namely the so-called fourth site.[16] Both interact with the side of the paddlewheel, in combination with the linkers themselves. In our structure however, there also appears to be interactions between the hydrogen on the linker as well, as seen for methane dosing in USTA-20.[18] Methane in the pores walls appears to be favoring the methane/phenyl interactions, unless there is steric hindrance from methane inside the pore; in which case the methane appears to favor paddlewheel/phenyl interactions.

For higher methane doses, Pawley refinements revealed that low angle backgrounds were not fitting effectively, when using the peak shape values from bare structure refinements. Upon further inspection, intensity appears absent for the low angle shoulders of the [111] and [311] peaks, which indicates that the symmetry forbidden [110] and [310] reflections are present (indicated by magenta asterisks in Figures S37 and S38), and inversion symmetry is absent in the higher gas loadings. Due to the higher gas loadings containing as many as nine crystallographically unique methane positions, lower symmetry refinements were not conducted. Instead initial refinements were conducted using a lower limit, and only final refinements involved the full data set. Further studies, focusing on the low angle regions are warranted to determine whether the absence of inversion symmetry is due to distortion of the pore, or uneven gas distribution in the material.

INS measurements conducted on bare PCN-81 are shown in Figure S50, along with 2 CH_4/Cu and 4 CH_4/Cu. The low energy peak, at 13 meV, corresponds with molecular libration, in agreement with INS on CH_4 dosed on MFM-300(In)[19], and highlighted by difference curves in Figure S50b. This peak increased with intensity as the materials is dosed with more CH_4, as expected for these types of vibrations. We additionally observe another feature above 160 meV, which is significantly broadened due to molecular recoil. The onset of this feature corresponds well with the calculated ν_4 bending mode for CH_4,[20] and appears blueshifted due to chemical interactions, also in agreement with simulations on CH_4 bound in clathrates.[20,21]

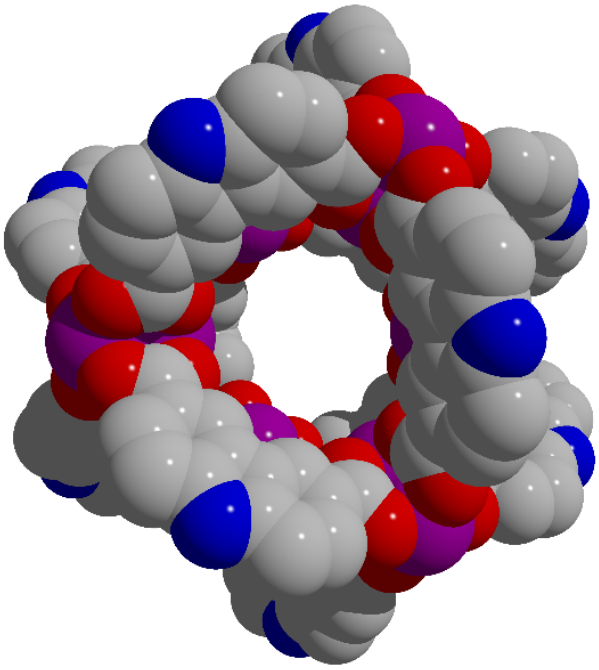

Figure S1. Single-crystal X-ray structure of $Cr_{12}(cdc)_{12}$ shown in a space-filling model. Purple, gray, red, and blue represent chromium, carbon, oxygen, and nitrogen, respectively. Hydrogen atoms and solvent have been omitted for clarity.

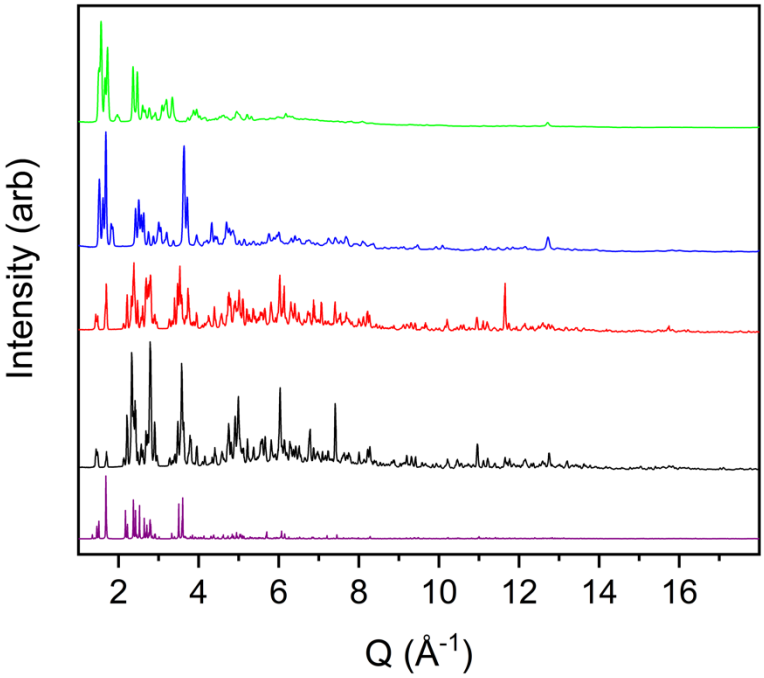

Figure S2. Powder X-ray diffraction patterns of as synthesized (black), DMF exchanged (red), MeOH exchanged (blue), and desolvated (green) $Cr_{12}(cdc)_{12}$ compared to the predicted (purple) powder pattern.

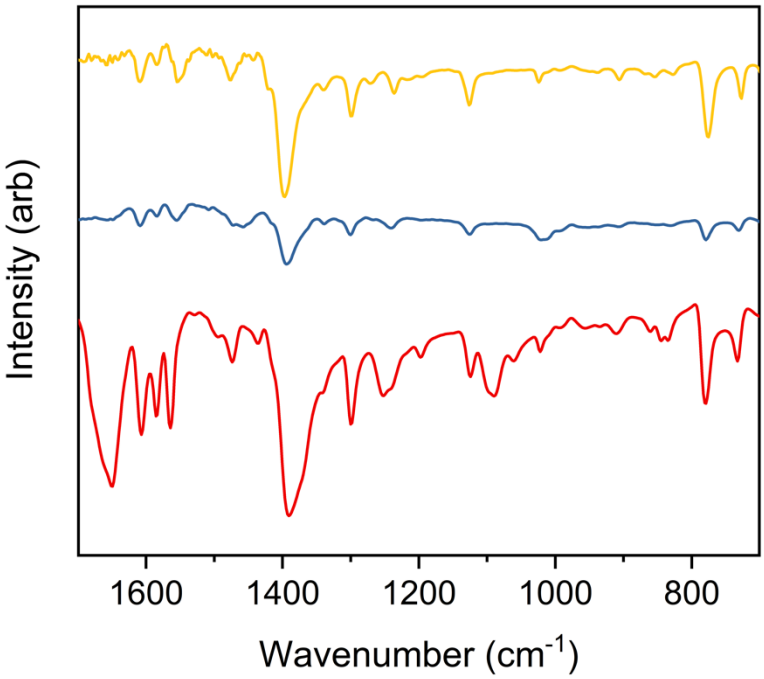

Figure S3. IR spectra of DMF exchanged (red), MeOH exchanged (blue), and desolvated (yellow) $Cr_{12}(cdc)_{12}$. Note the lack of amide stretch (DMF) upon activation.

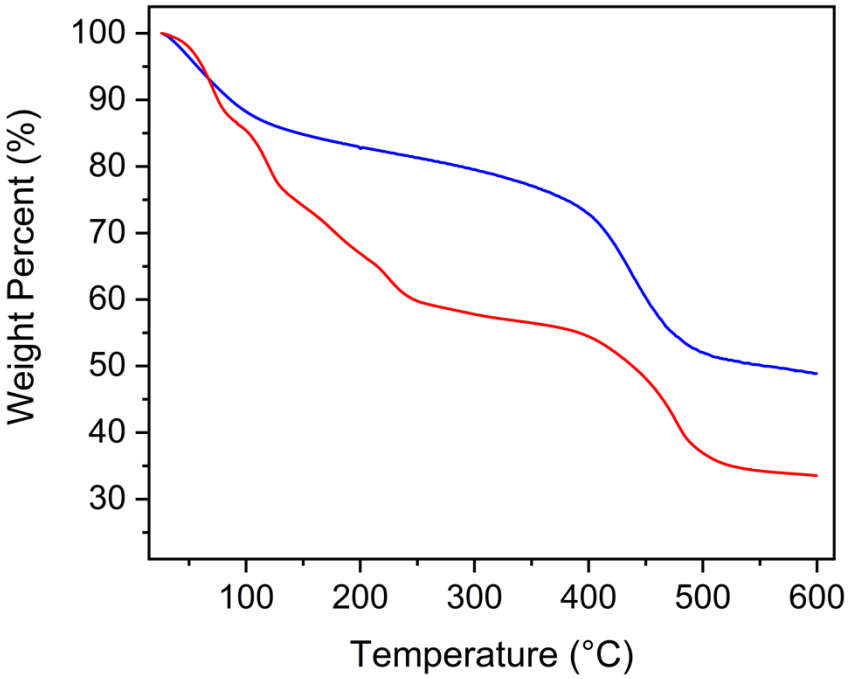

Figure S4. Thermogravimetric analysis of DMF exchanged (red) and MeOH exchanged (blue) $Cr_{12}(cdc)_{12}$ from 50 °C to 600 °C with a ramp rate of 2 degrees per minute.

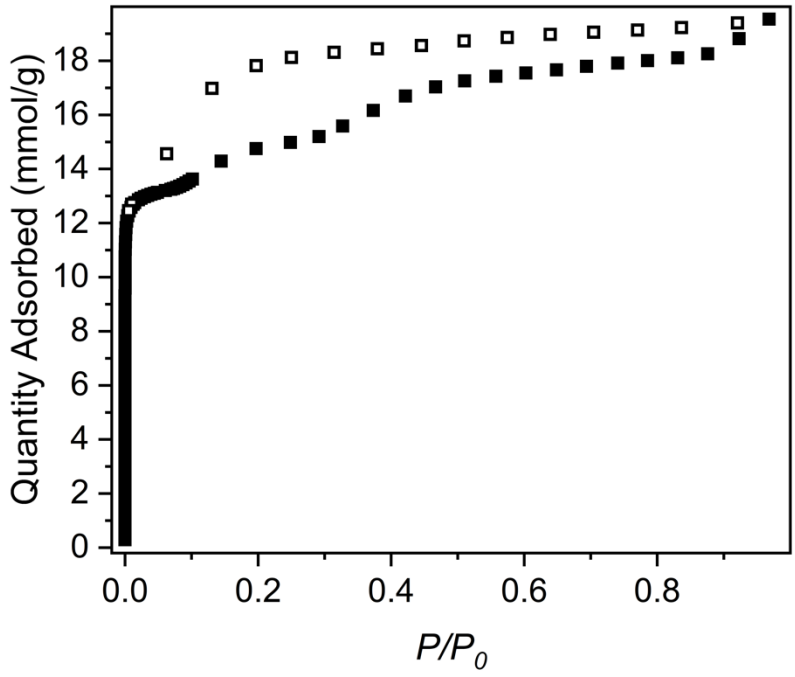

Figure S5. N_2 adsorption in $Cr_{12}(cdc)_{12}$ at 77 K. Filled and open symbols represent adsorption and desorption, respectively.

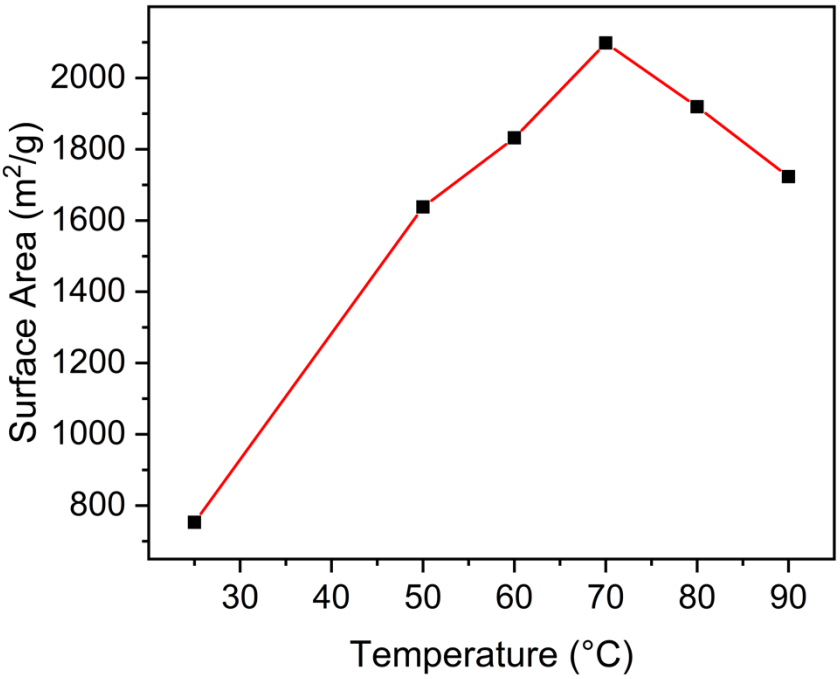

Figure S6. Surface area as a function of activation temperature for $Cr_{12}(cdc)_{12}$. The sample was heated at each temperature until the static off-gas rate was below 2 μbar/min.

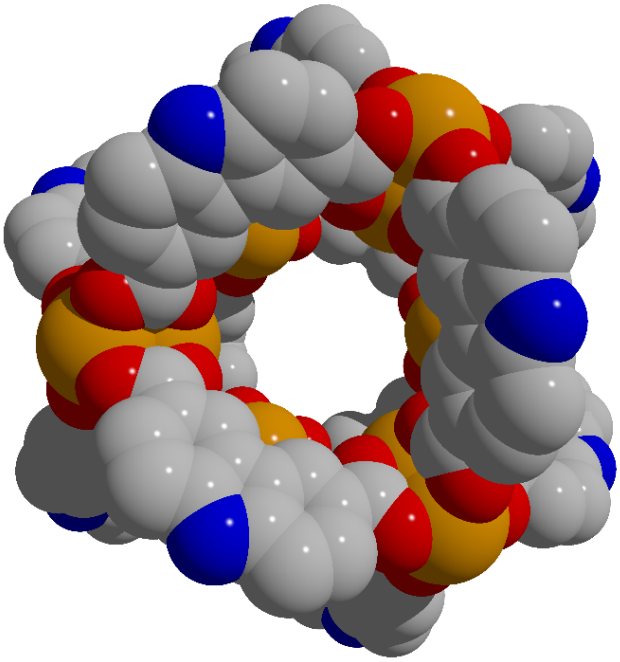

Figure S7. Single crystal X-ray structure of $Mo_{12}(cdc)_{12}$ shown in a space-filling model. Orange, gray, red and blue represent molybdenum, carbon, oxygen and nitrogen, respectively. Hydrogen atoms and solvent have been omitted for clarity.

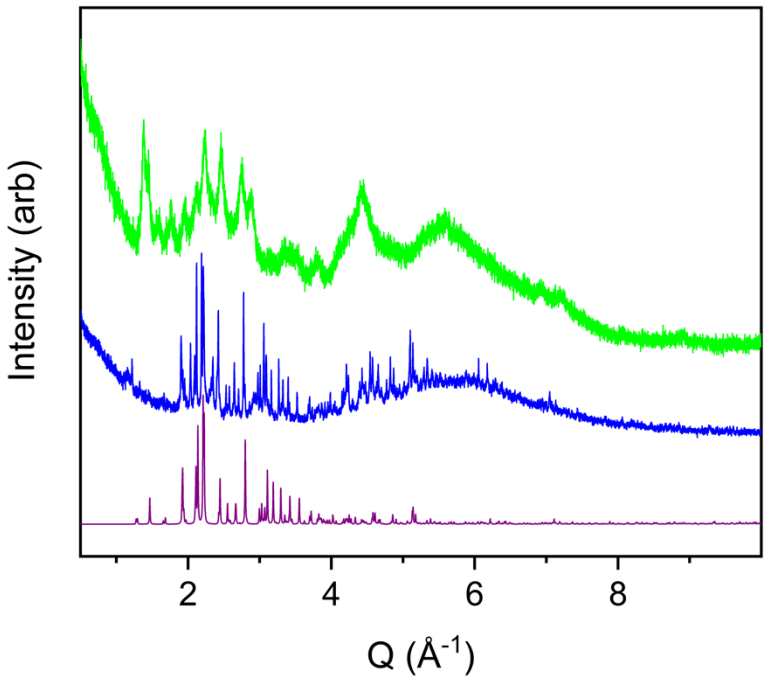

Figure S8. Powder X-ray diffraction patterns of MeOH exchanged (blue) and desolvated (green) $Mo_{12}(cdc)_{12}$ as compared to the predicted pattern (purple).

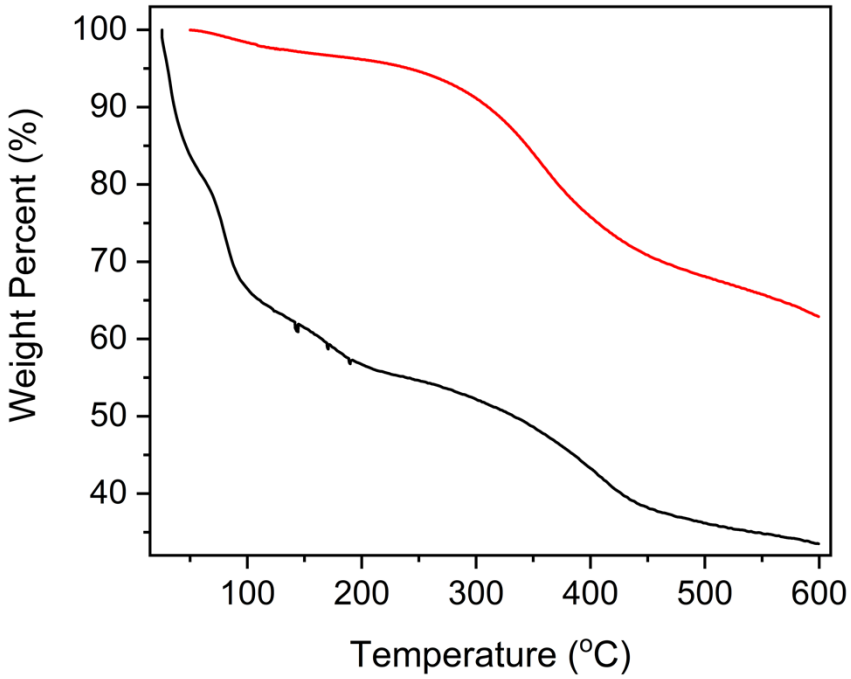

Figure S9. Thermogravimetric analysis of as synthesized (black) and MeOH exchanged (red) $Mo_{12}(cdc)_{12}$ from 50 °C to 600 °C with a ramp rate of 2 degrees per minute.

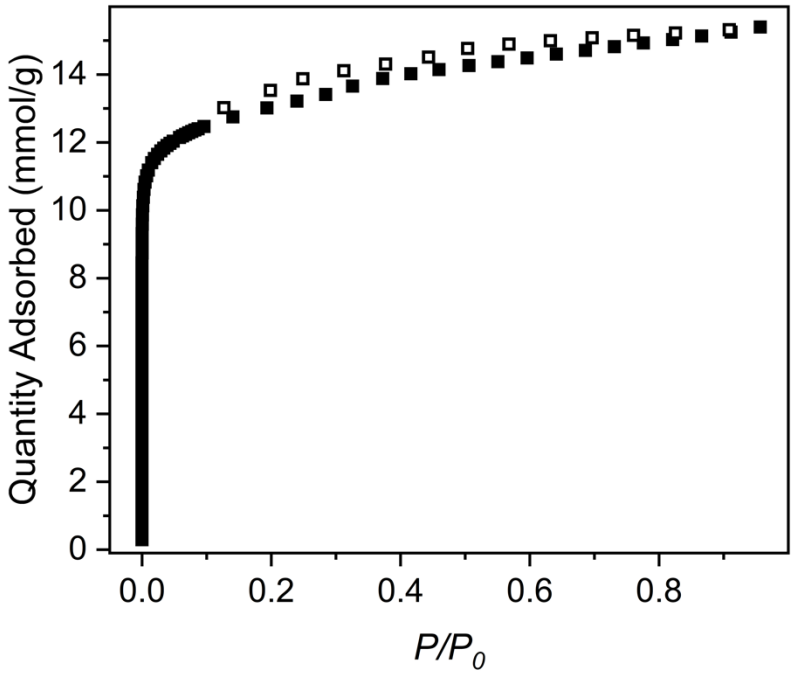

Figure S10. N_2 adsorption in $Mo_{12}(cdc)_{12}$ at 77 K. Filled and open symbols represent adsorption and desorption, respectively.

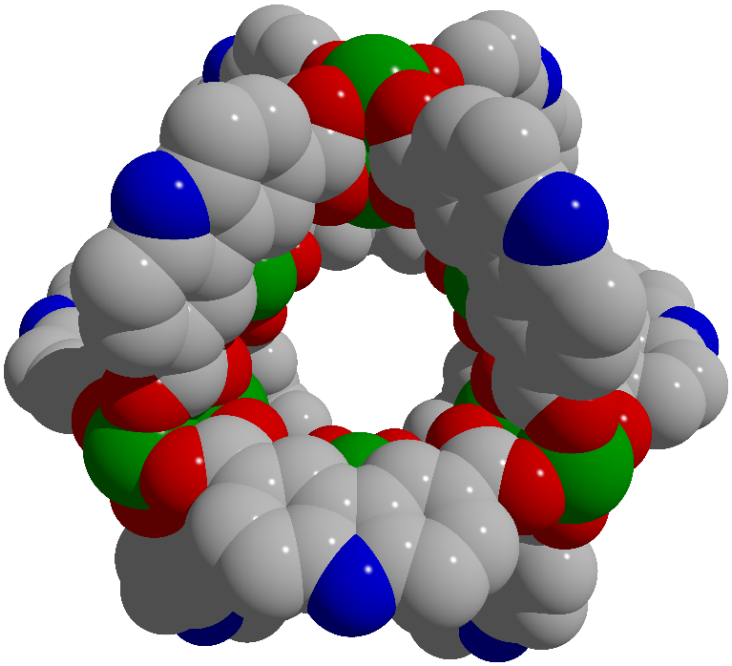

Figure S11. Single crystal X-ray structure of $Cu_{12}(cdc)_{12}$ shown in a space-filling model. Green, gray, red and blue represent copper, carbon, oxygen and nitrogen, respectively. Hydrogen atoms and solvent have been omitted for clarity.

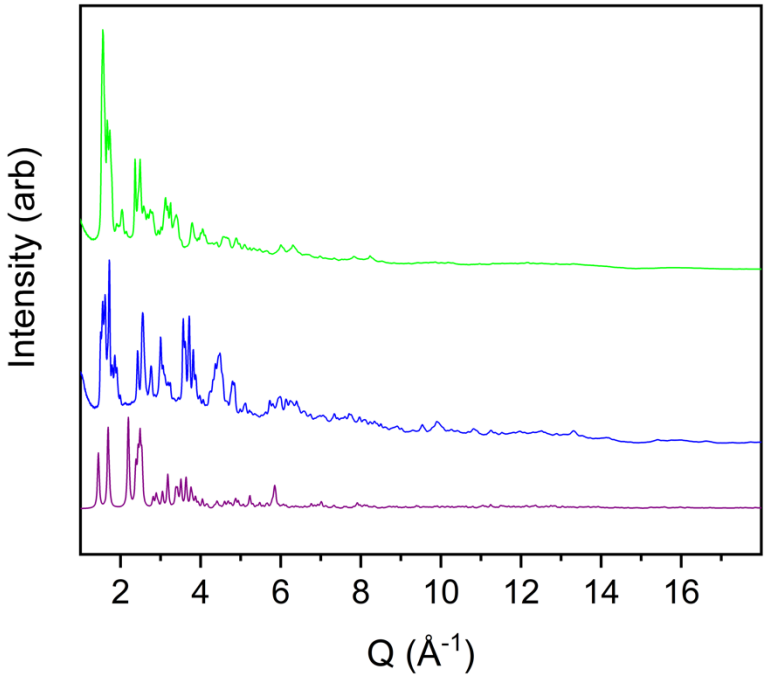

Figure S12. Powder X-ray diffraction patterns of MeOH exchanged (blue) and desolvated (green) $Cu_{12}(cdc)_{12}$ as compared to the predicted pattern (purple).

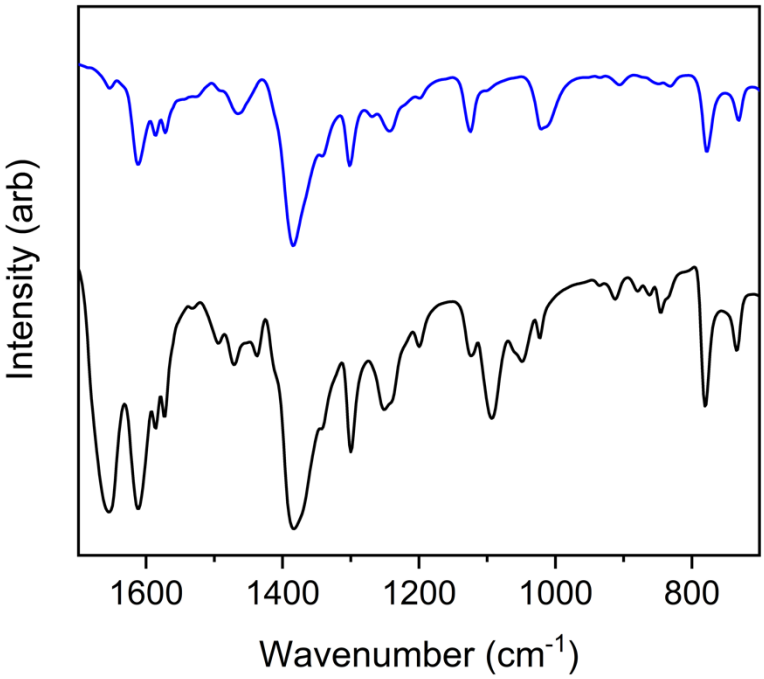

Figure S13. IR spectra of as synthesized (black) and MeOH exchanged (blue) $Cu_{12}(cdc)_{12}$.

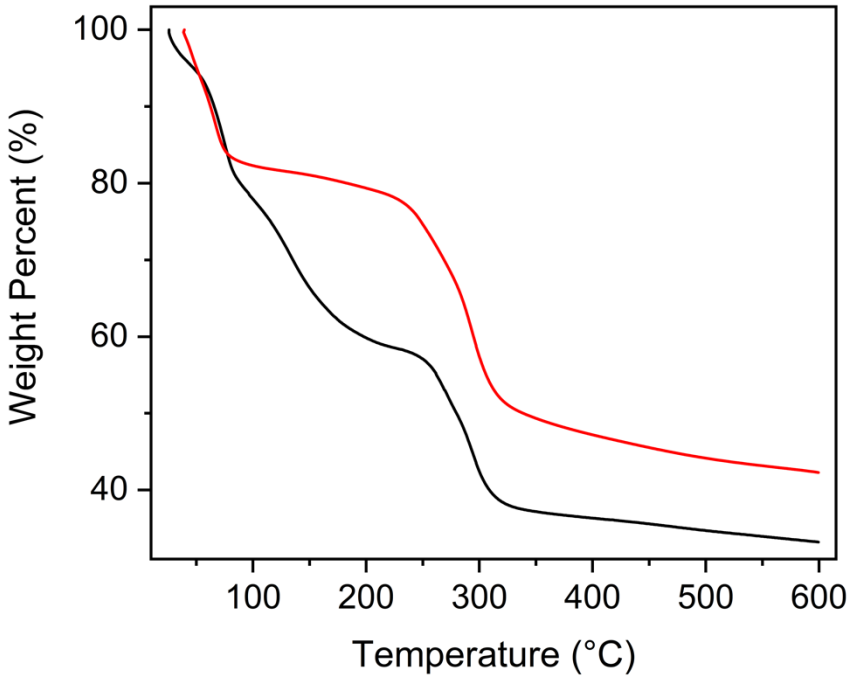

Figure S14. Thermogravimetric analysis of as synthesized (black) and MeOH exchanged (red) $Cu_{12}(cdc)_{12}$ from 50 °C to 600 °C with a ramp rate of 2 degrees per minute.

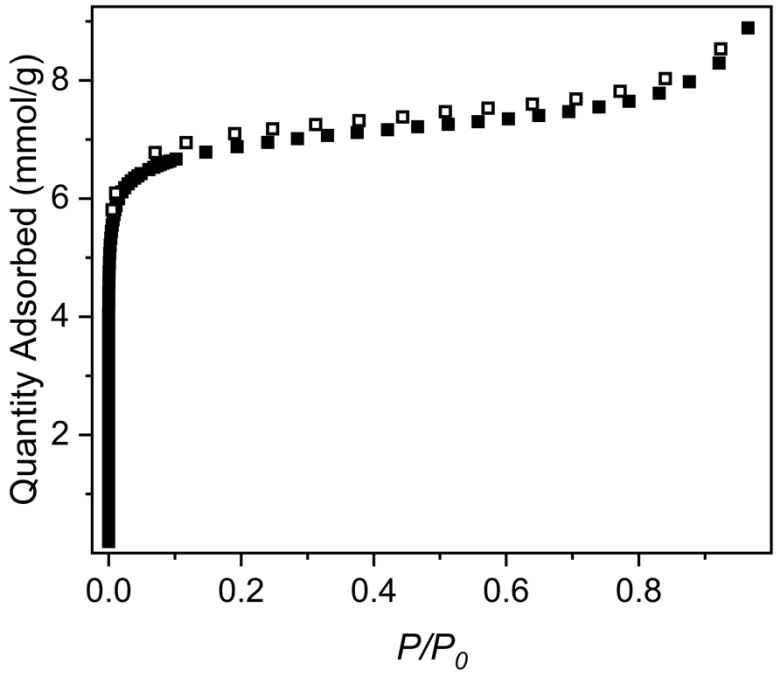

Figure S15. N_2 adsorption in $Cu_{12}(cdc)_{12}$ at 77 K. Filled and open symbols represent adsorption and desorption, respectively.

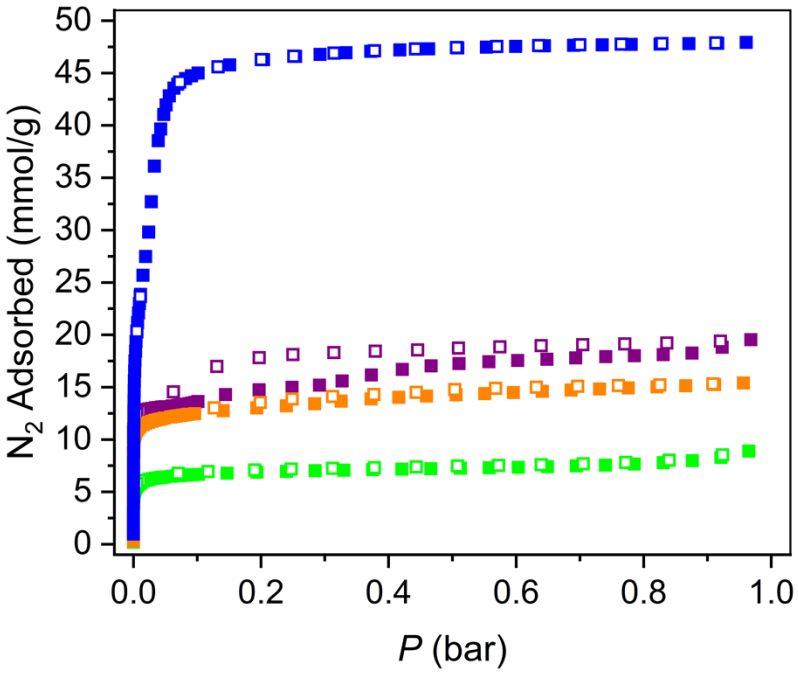

Figure S16. N_2 adsorption in $Cu_{12}(cdc)_{12}$ (green), $Mo_{12}(cdc)_{12}$ (orange), $Cr_{12}(cdc)_{12}$ (purple), and PCN-81 (blue) at 77 K. Filled and open symbols represent adsorption and desorption, respectively.

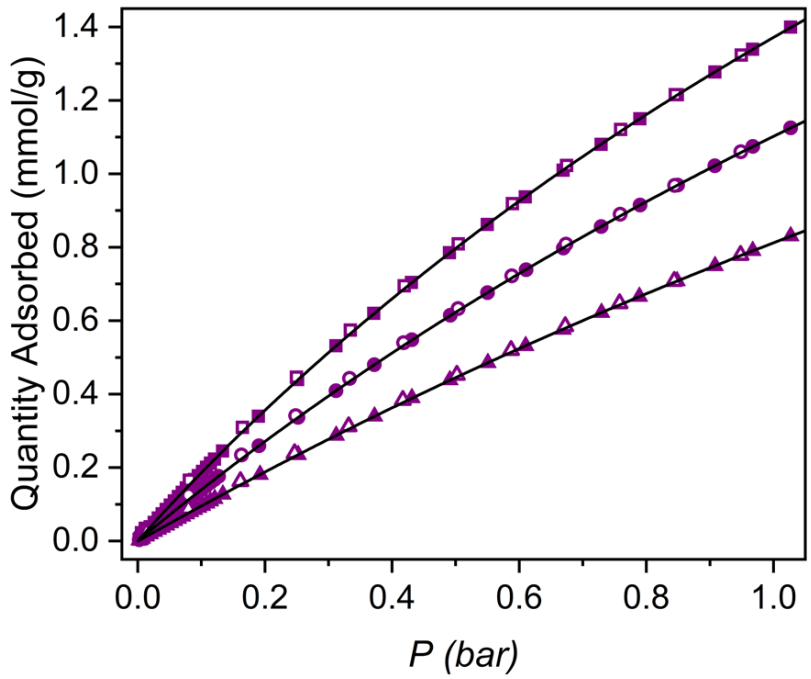

Figure S17. Low-pressure methane adsorption in $Cr_{12}(cdc)_{12}$ at 273 (squares), 283 (circles) and 298 (triangles). Filled and open symbols represent adsorption and desorption, respectively. The black lines are the respective single-site Langmuir-Freundlich fits using the parameters in **Table S1**.

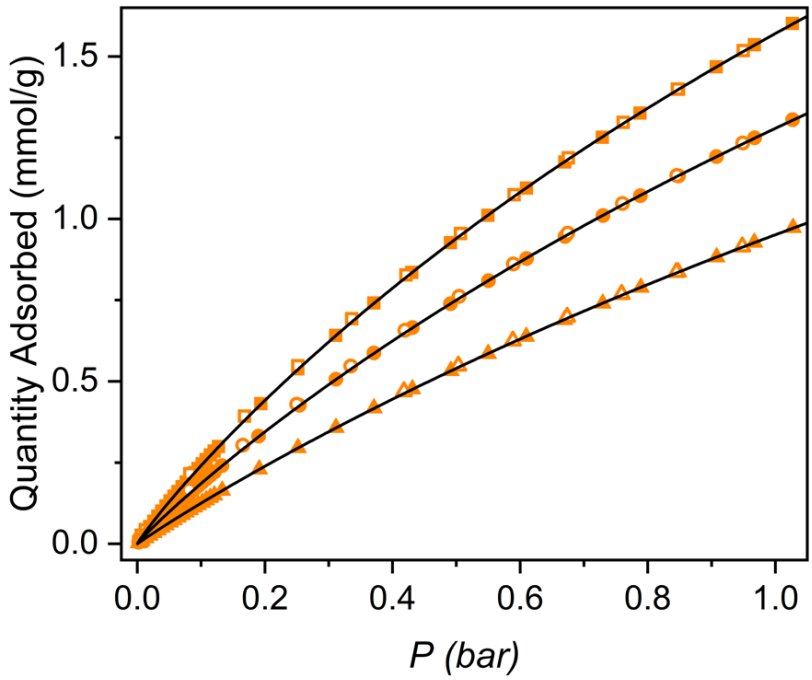

Figure S18. Low-pressure methane adsorption in $Mo_{12}(cdc)_{12}$ at 273 (squares), 283 (circles) and 298 (triangles). Filled and open symbols represent adsorption and desorption, respectively. The black lines are the respective single-site Langmuir-Freundlich fits using the parameters in **Table S1**.

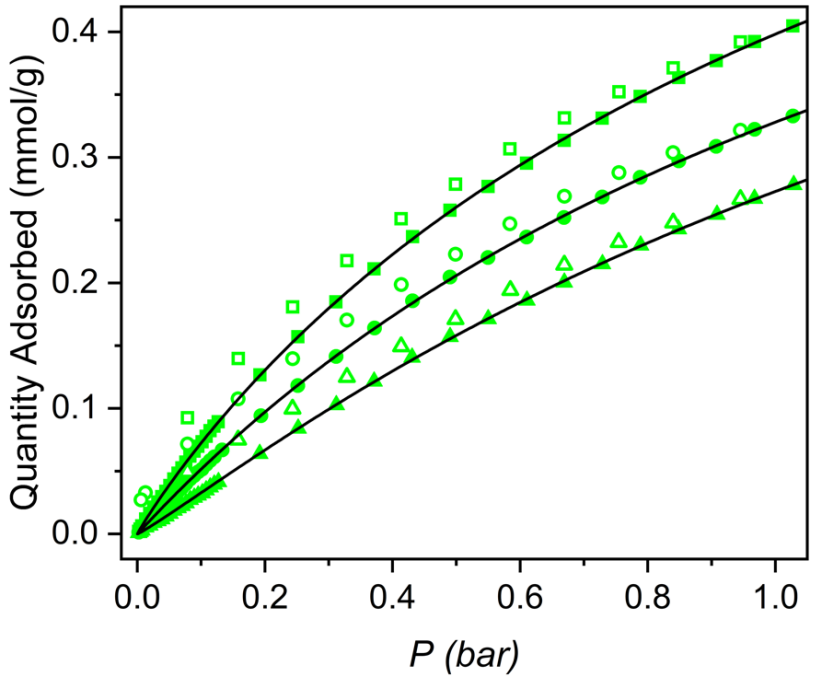

Figure S19. Low-pressure methane adsorption in $Cu_{12}(cdc)_{12}$ at 273 (squares), 283 (circles) and 298 (triangles). Filled and open symbols represent adsorption and desorption, respectively. The black lines are the respective single-site Langmuir-Freundlich fits using the parameters in **Table S1**.

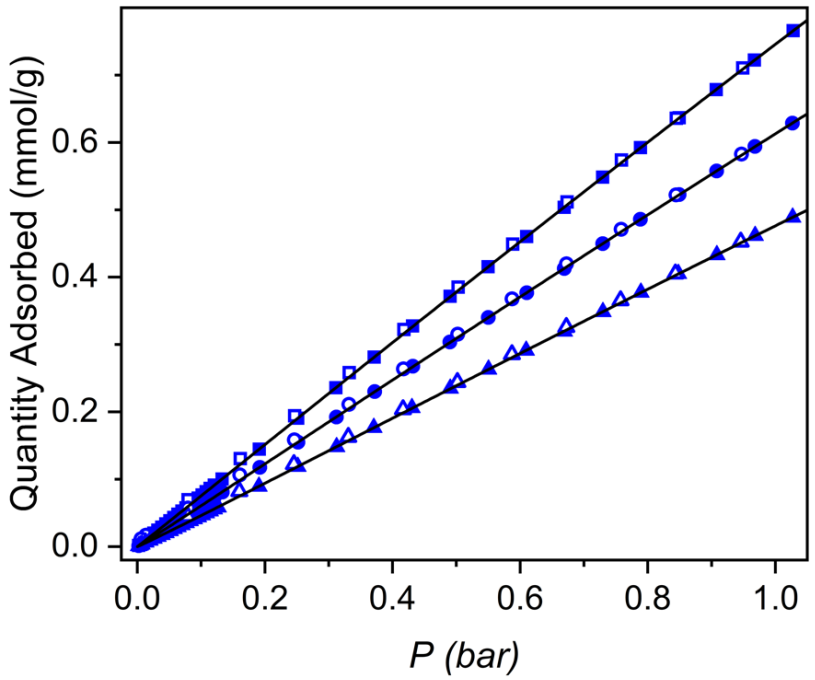

Figure S20. Low-pressure methane adsorption in PCN-81 at 273 (squares), 283 (circles) and 298 (triangles). Filled and open symbols represent adsorption and desorption, respectively. The black lines are the respective single-site Langmuir-Freundlich fits using the parameters in **Table S1**.

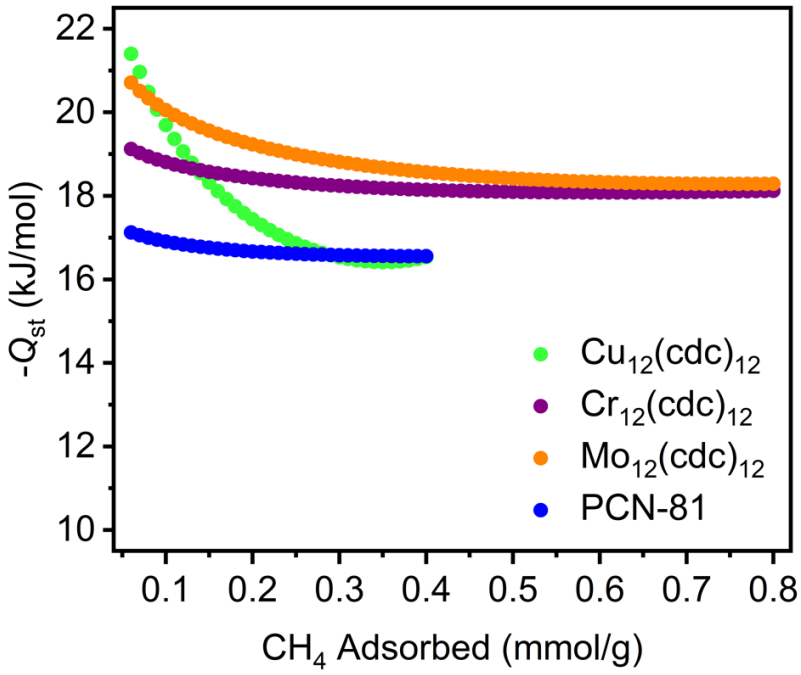

Figure S21. Methane adsorption enthalpy as a function of loading for the four porous materials.

Table S1. Summary of Langmuir-Freundlich parameters for $Cr_{12}(cdc)_{12}$, $Mo_{12}(cdc)_{12}$, $Cu_{12}(cdc)_{12}$ and PCN-81.

	$Cr_{12}(cdc)_{12}$			$Mo_{12}(cdc)_{12}$			$Cu_{12}(cdc)_{12}$			PCN-81		
	273	283	298	273	283	298	273	283	298	273	283	298
$q_{sat,1}$	5.229	4.927	4.403	6.282	5.615	4.675	0.923	0.803	0.755	16.571	12.295	9.435
b_1	0.356	0.288	0.226	0.333	0.295	0.256	0.759	0.691	0.566	0.047	0.055	0.053
v_1	0.983	0.993	1.008	0.922	0.935	0.967	0.949	1.002	1.094	1.013	1.024	1.033

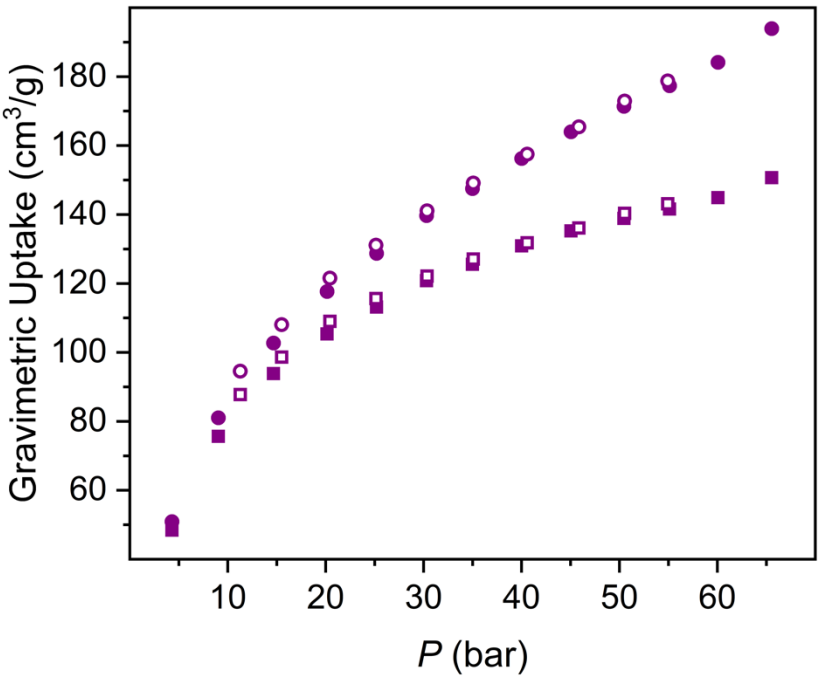

Figure S22. High-pressure excess (squares) and total (circles) methane adsorption in $Cr_{12}(cdc)_{12}$ at 298 K. Filled and open symbols represent adsorption and desorption, respectively.

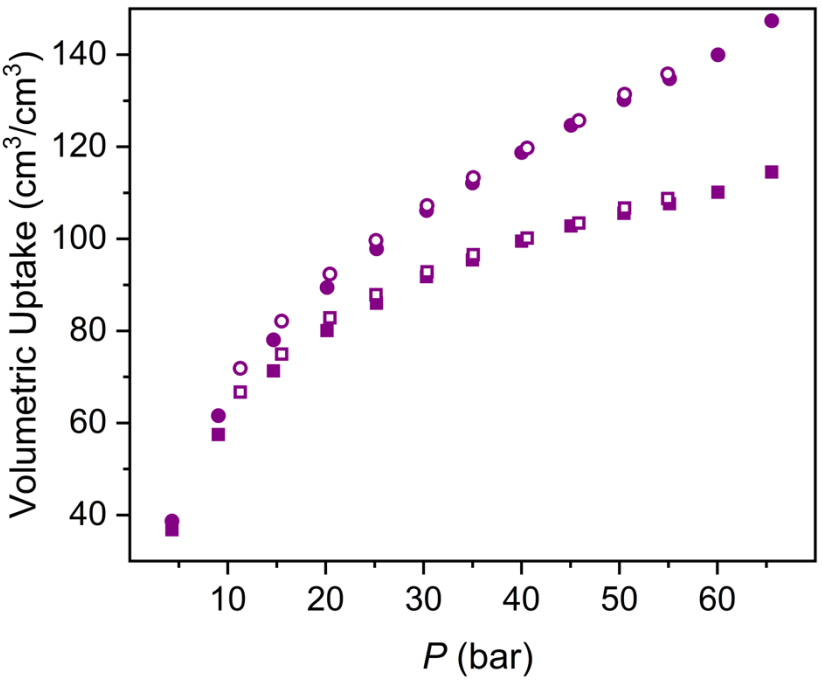

Figure S23. High-pressure excess (squares) and total (circles) methane adsorption in $Cr_{12}(cdc)_{12}$ at 298 K. Filled and open symbols represent adsorption and desorption, respectively.

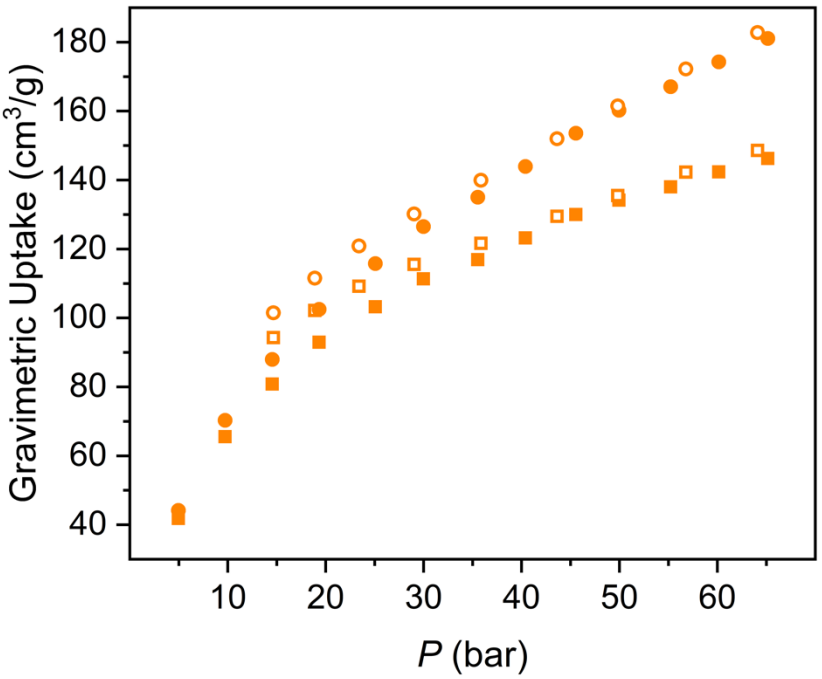

Figure S24. High-pressure excess (squares) and total (circles) methane adsorption in $Mo_{12}(cdc)_{12}$ at 298 K. Filled and open symbols represent adsorption and desorption, respectively.

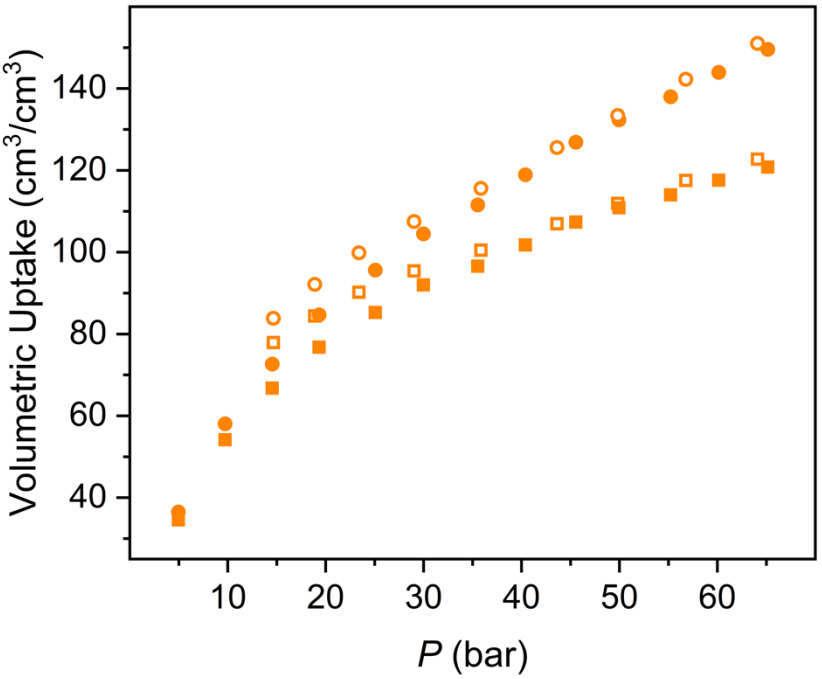

Figure S25. High-pressure excess (squares) and total (circles) methane adsorption in $Mo_{12}(cdc)_{12}$ at 298 K. Filled and open symbols represent adsorption and desorption, respectively.

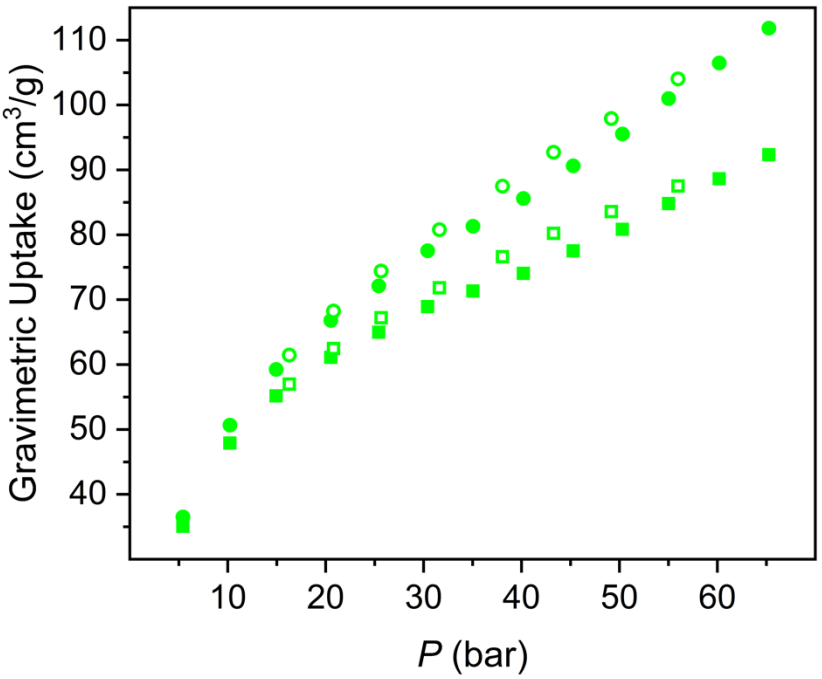

Figure S26. High-pressure excess (squares) and total (circles) methane adsorption in $Cu_{12}(cdc)_{12}$ at 298 K. Filled and open symbols represent adsorption and desorption, respectively.

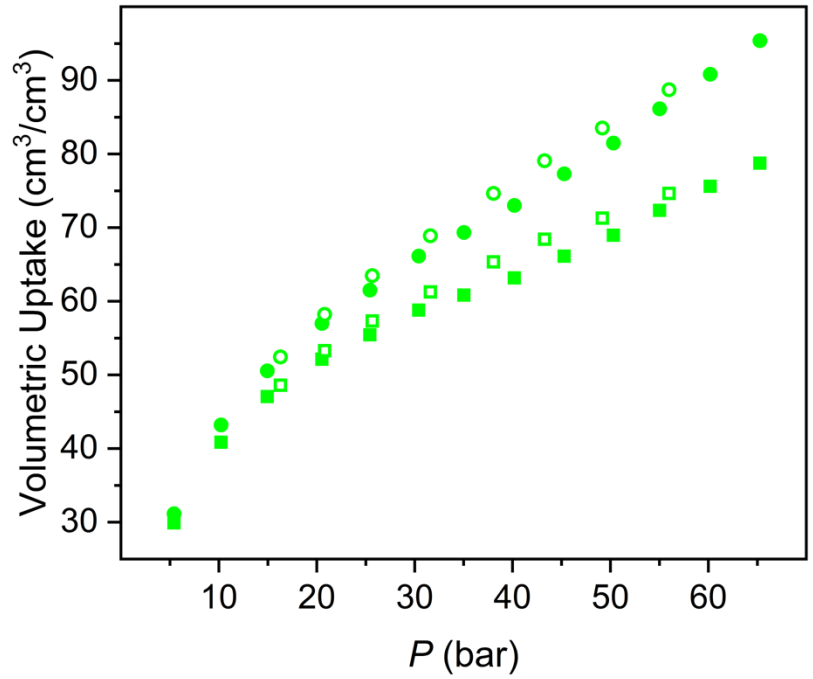

Figure S27. High-pressure excess (squares) and total (circles) methane adsorption in $Cu_{12}(cdc)_{12}$ at 298 K. Filled and open symbols represent adsorption and desorption, respectively.

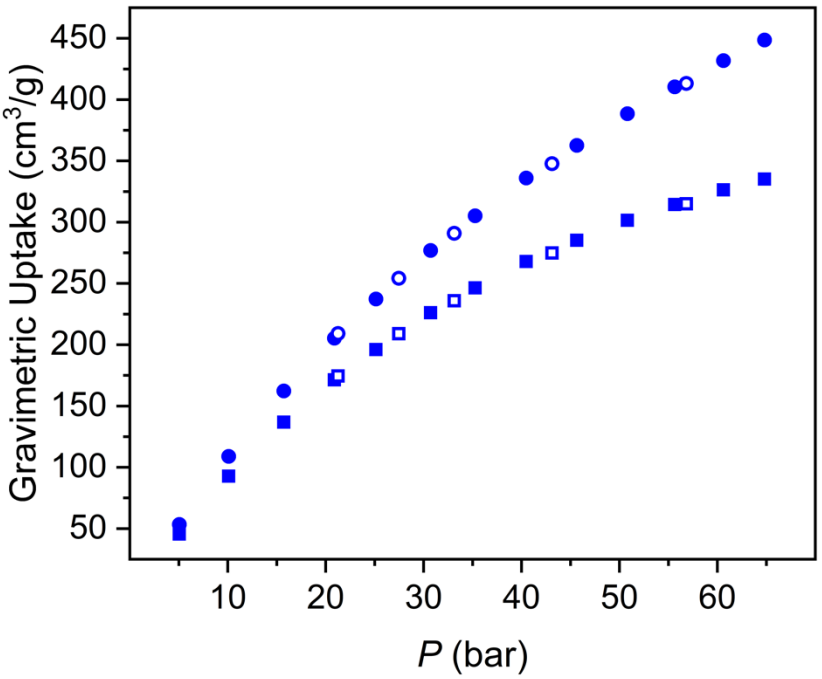

Figure S28. High-pressure excess (squares) and total (circles) methane adsorption in PCN-81 at 298 K. Filled and open symbols represent adsorption and desorption, respectively.

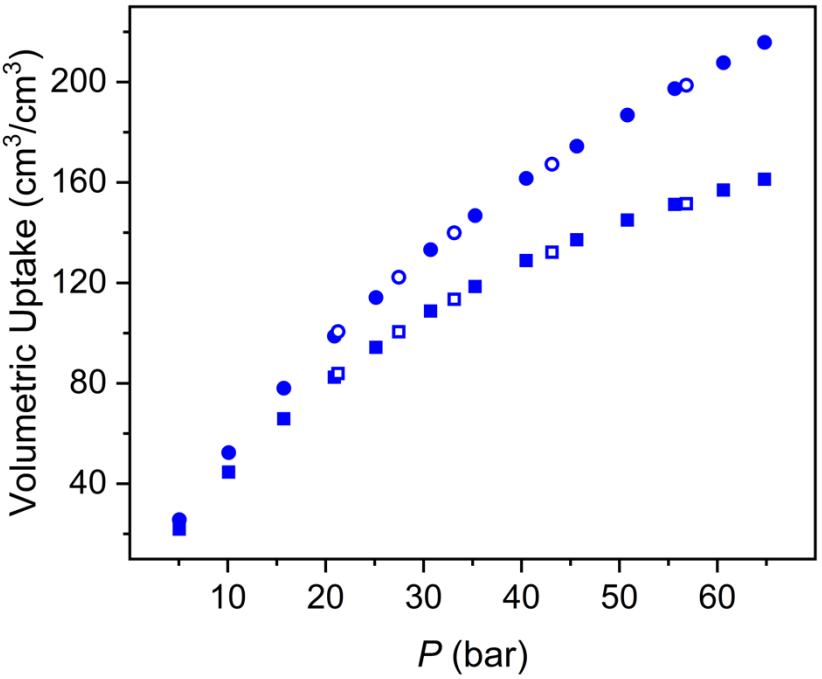

Figure S29. High-pressure excess (squares) and total (circles) methane adsorption in PCN-81 at 298 K. Filled and open symbols represent adsorption and desorption, respectively.

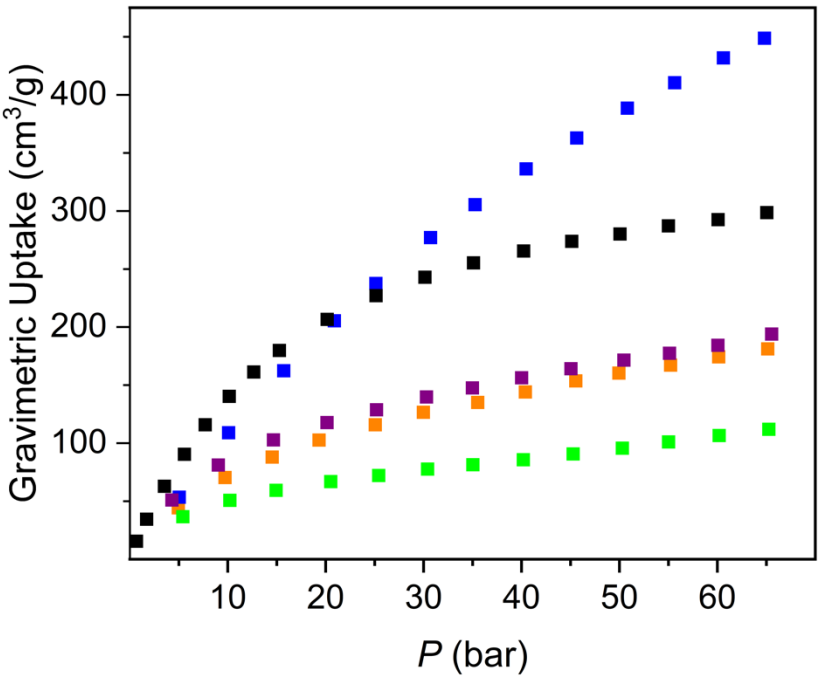

Figure S30. High-pressure total methane adsorption in $Cu_{12}(cdc)_{12}$ (green), $Mo_{12}(cdc)_{12}$ (orange), $Cr_{12}(cdc)_{12}$ (purple), HKUST-1 (black), and PCN-81 (blue) at 298 K.

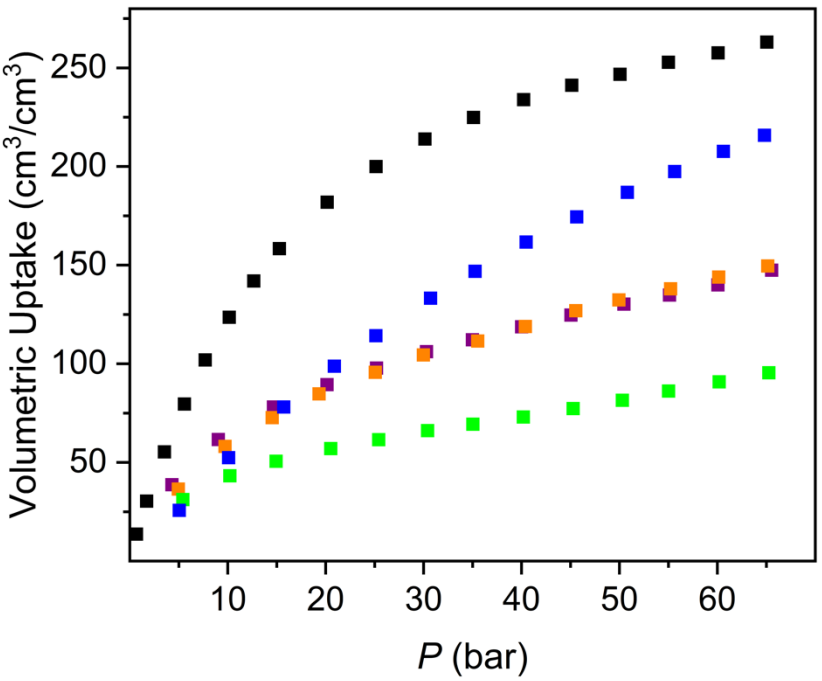

Figure S31. High-pressure total methane adsorption in $Cu_{12}(cdc)_{12}$ (green), $Mo_{12}(cdc)_{12}$ (orange), $Cr_{12}(cdc)_{12}$ (purple), HKUST-1 (black), and PCN-81 (blue) at 298 K.

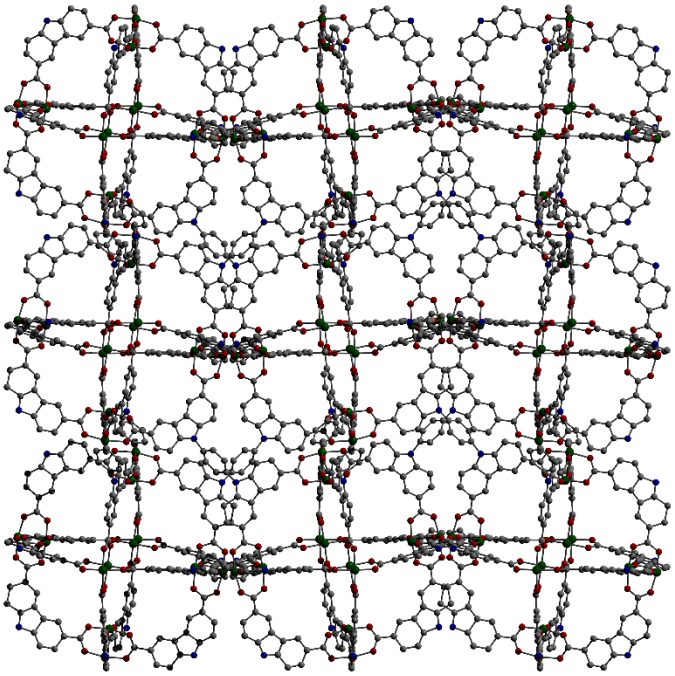

Figure S32. PCN-81 X-ray crystal structure view along the a-axis with H-atoms omitted for clarity.

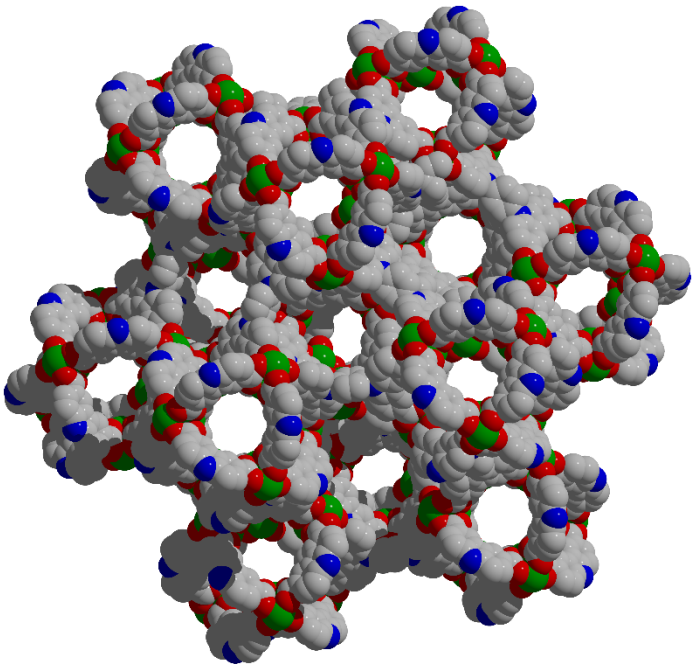

Figure S33. A portion of the PCN-81 X-ray crystal structure shown in a space-filling model with H-atoms omitted for clarity.

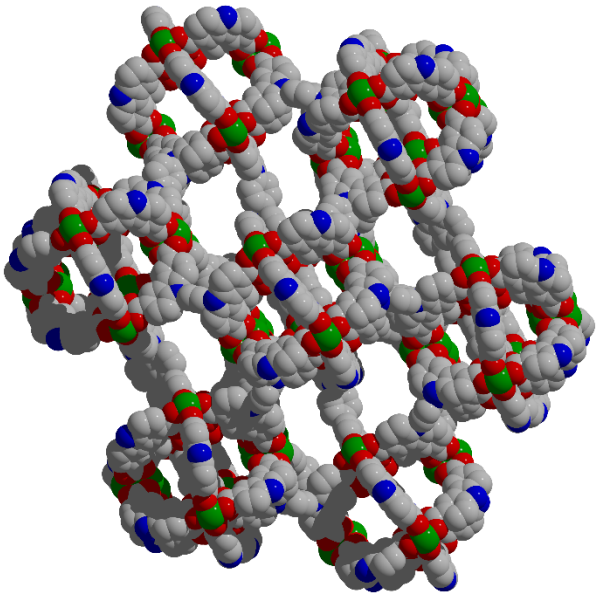

Figure S34. A portion of the PCN-81 X-ray crystal structure shown in a space-filling model with H-atoms omitted for clarity.

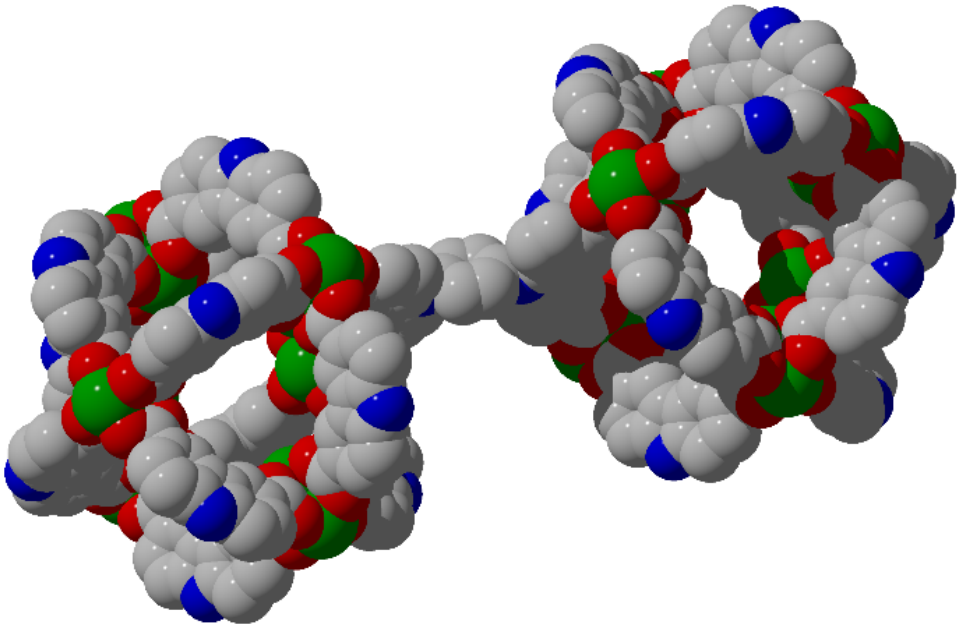

Figure S35. Two carbazole-based cages of PCN-81 illustrating their isostructural nature to $M_{12}(cdc)_{12}$ cages.

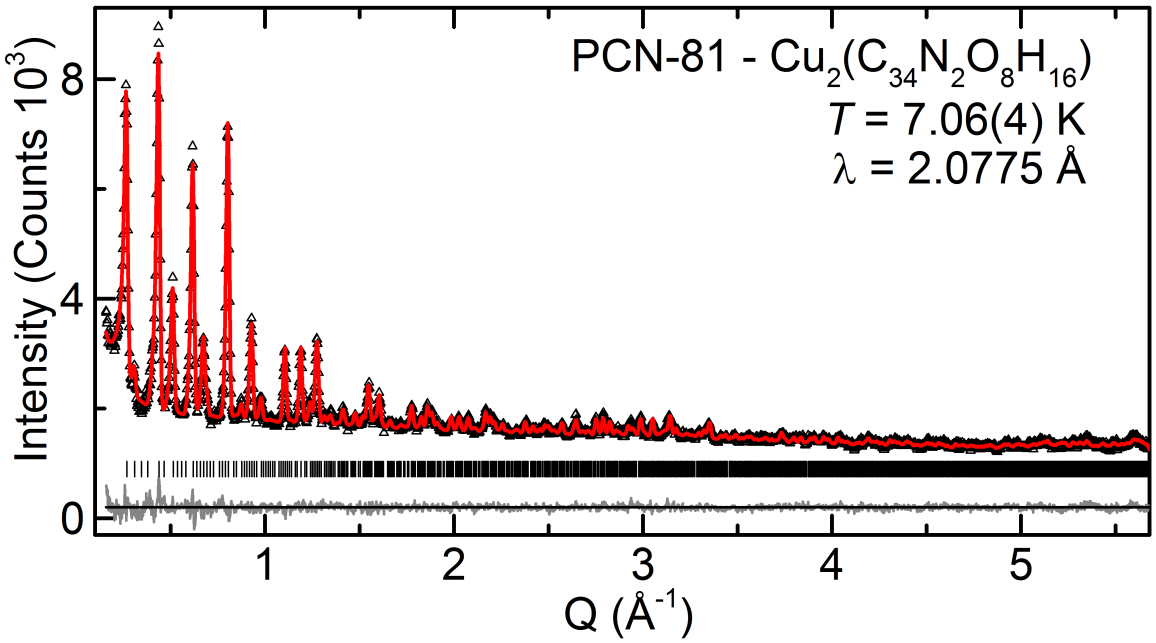

Figure S36. Rietveld refinement of activated PCN-81 powder neutron diffraction data, using spacegroup (*Pa*-3) (black ticks, a = 40.520(2) Å). Experimental data shown as black triangles, fit in red, with difference curve in gray. Symbols are commensurate with error bars (which indicate one standard deviation). Fit statistics were R_{wp} = 2.81%, R_p = 2.35%, and GoF = 1.10.

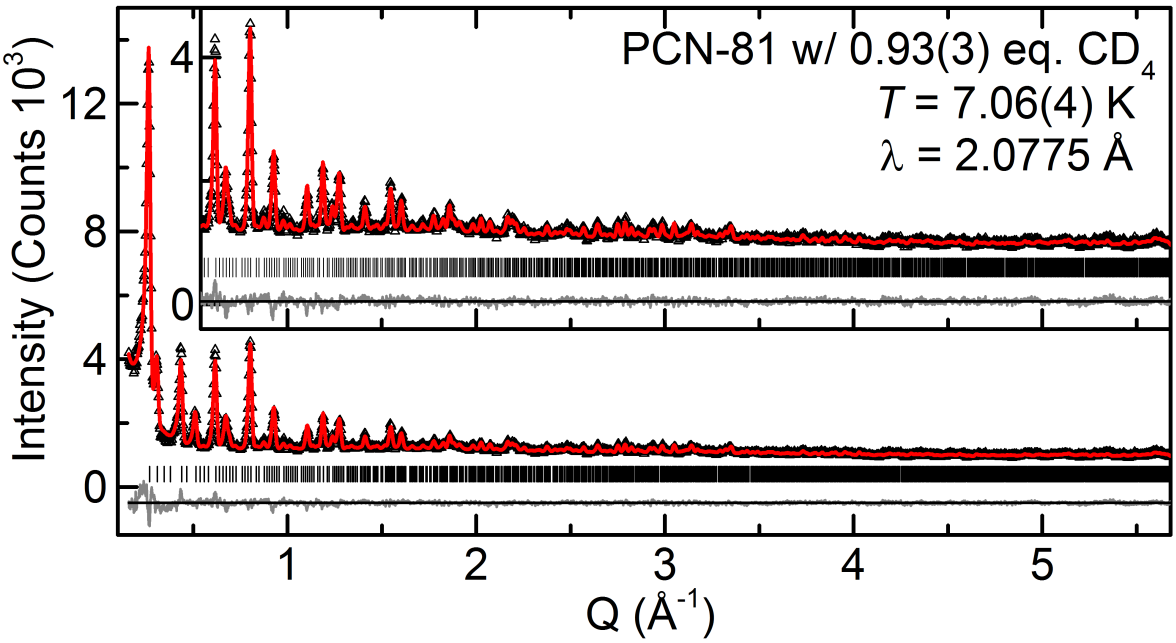

Figure S37. Rietveld refinement of PCN-81 powder neutron diffraction data, using space group (*Pa*-3) (black ticks, a = 40.520(2) Å). Experimental data shown as black triangles, fit in red, with difference curve in gray. Symbols are commensurate with error bars (which indicate one standard deviation). Fit statistics were R_{wp} = 3.38%, R_p = 3.00%, and GoF = 1.12.

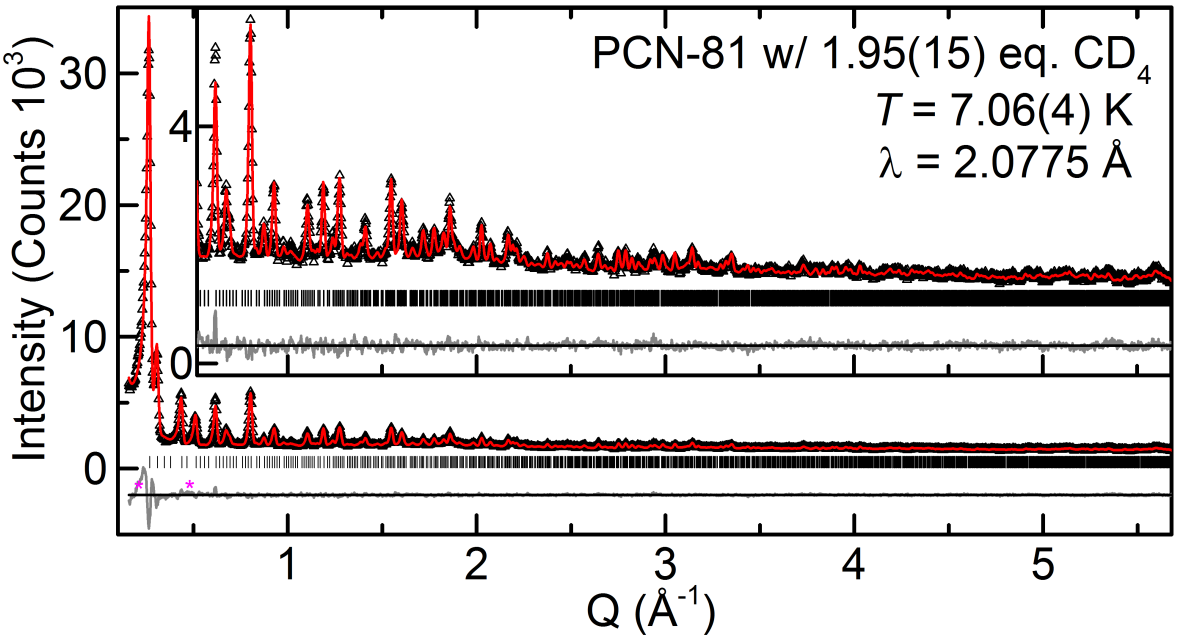

Figure S38. Rietveld refinement of PCN-81 powder neutron diffraction data, using space group (*Pa*-3) (black ticks, a = 40.519(2) Å). Experimental data shown as black triangles, fit in red, with difference curve in gray. Symbols are commensurate with error bars (which indicate one standard deviation). Fit statistics were R_{wp} = 3.20%, R_p = 3.11%, and GoF = 1.30.

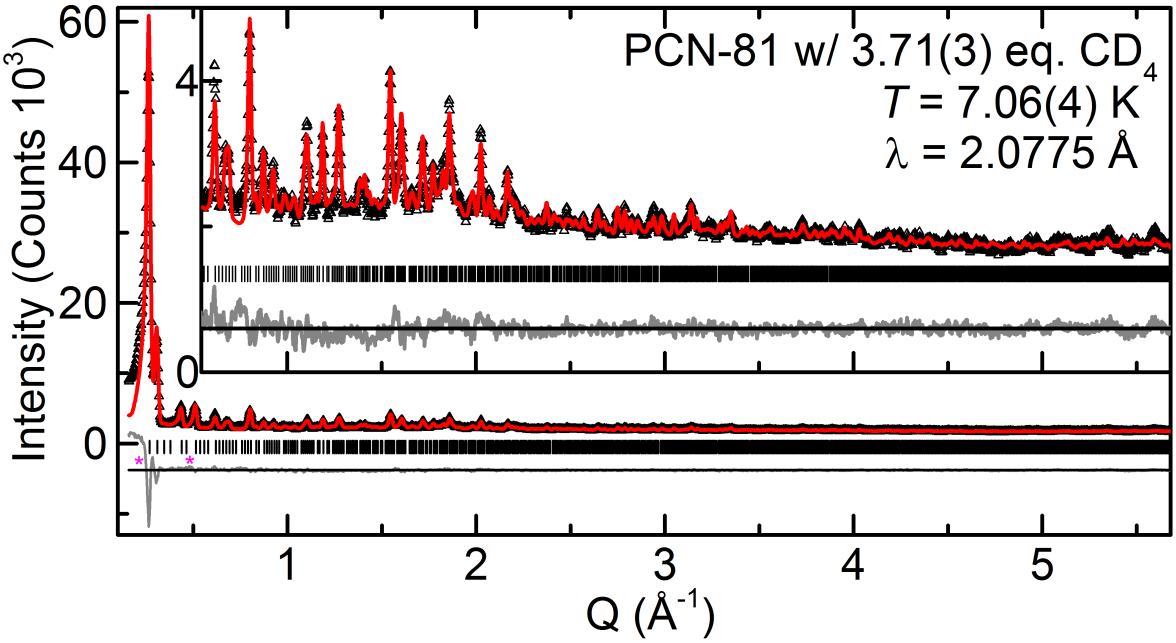

Figure S39. Rietveld refinement of activated PCN-81 powder neutron diffraction data, using space group (*Pa*-3) (black ticks, a = 40.530(4) Å). Experimental data shown as black triangles, fit in red, with difference curve in gray. Symbols are commensurate with error bars (which indicate one standard deviation). Fit statistics were R_{wp} = 6.26%, R_p = 5.67%, and GoF = 2.80.

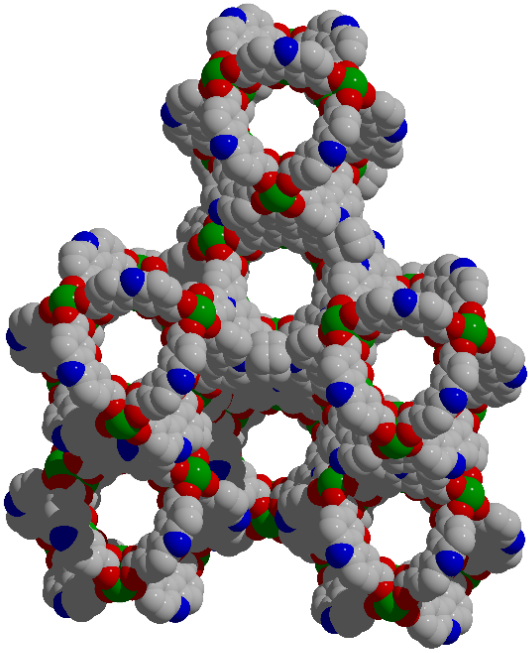

Figure S40. Activated PCN-81 structure solved via powder neutron diffraction shown in a space filling model with H-atoms omitted for clarity. Green, gray, red, and blue represent copper, carbon, oxygen, and nitrogen respectively.

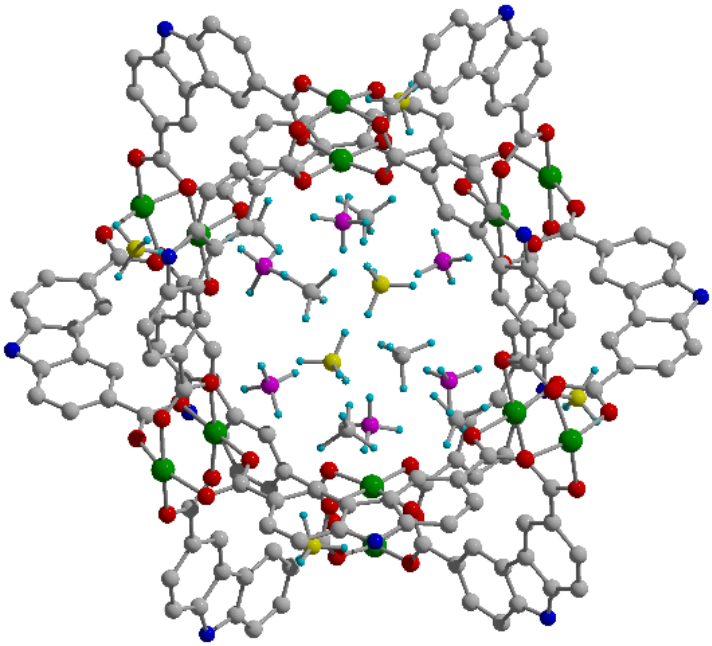

Figure S41. PCN-81 dosed with 0.93 equivalents of CD_4 per metal center solved via powder neutron diffraction with H-atoms omitted for clarity. Green, gray, red, and blue represent copper, carbon, oxygen, and nitrogen respectively.

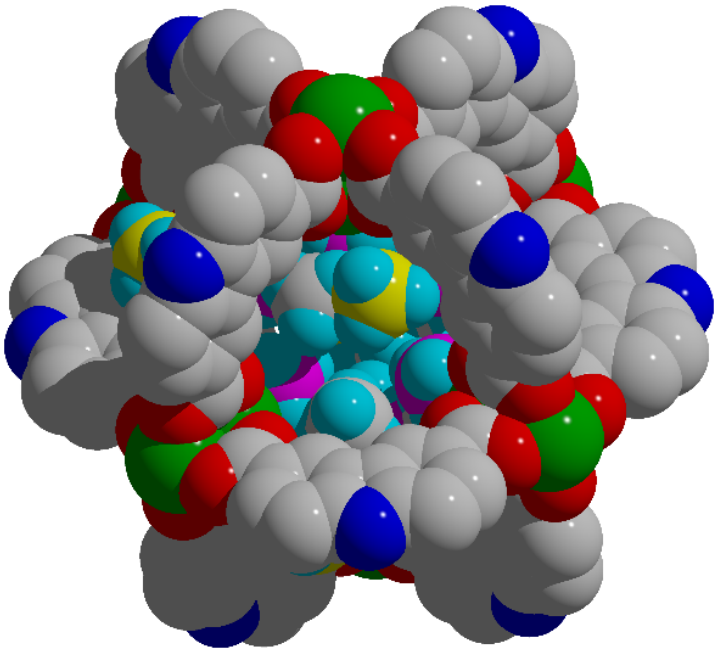

Figure S42. PCN-81 dosed with 0.93 equivalents of CD_4 per metal center solved via powder neutron diffraction shown in a space-filling model with H-atoms omitted for clarity. Green, gray, red, and blue represent copper, carbon, oxygen, and nitrogen respectively.

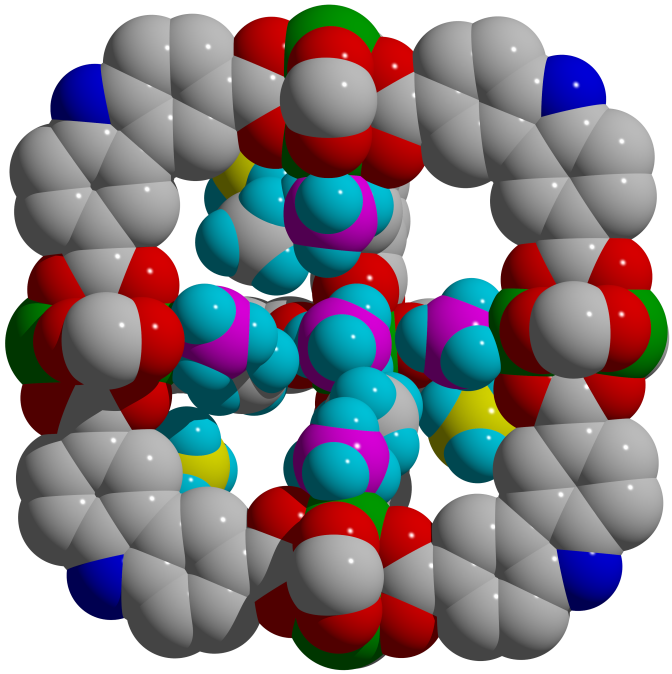

Figure S43. Space-filling representation of CD_4 adsorbed on the interior of the carbazole-based cage of PCN-81.

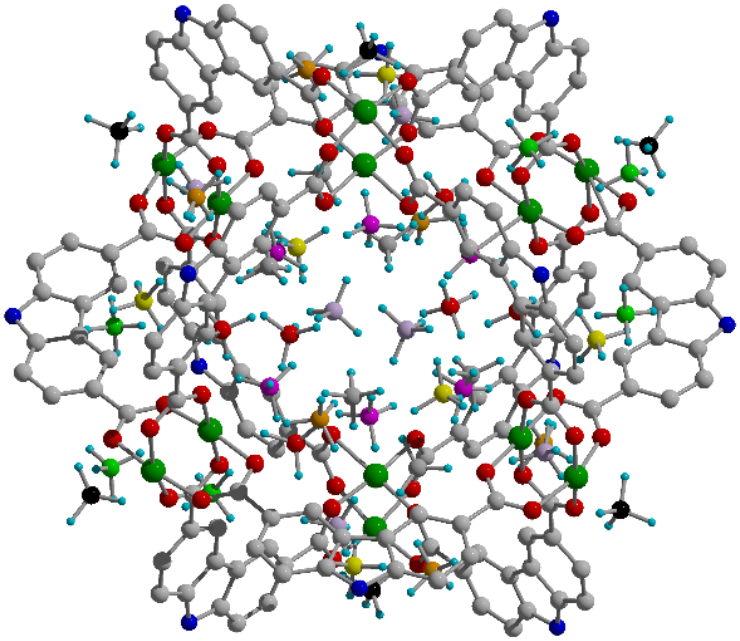

Figure S44. PCN-81 dosed with 1.95 equivalents of CD_4 per metal center solved via powder neutron diffraction with H-atoms omitted for clarity. Green, gray, red, and blue represent copper, carbon, oxygen, and nitrogen respectively.

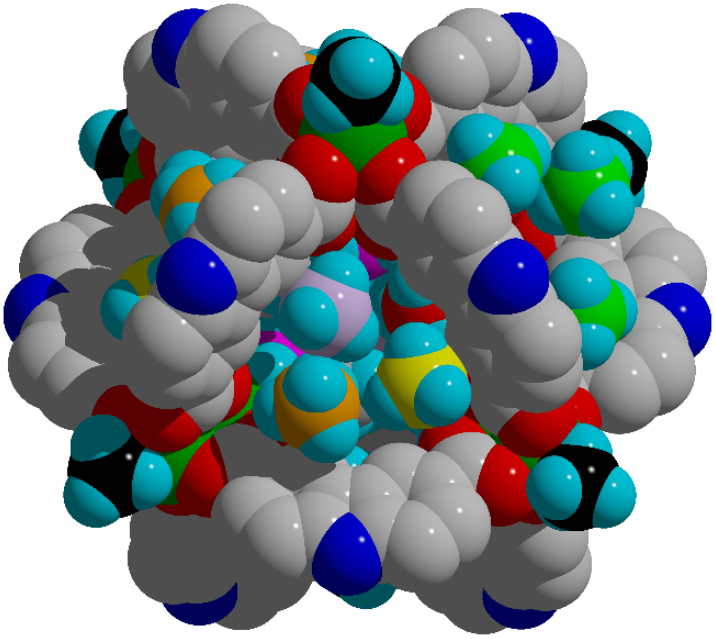

Figure S45. PCN-81 dosed with 1.95 equivalents of CD_4 per metal center solved via powder neutron diffraction shown in a space-filling model with H-atoms omitted for clarity. Green, gray, red, and blue represent copper, carbon, oxygen, and nitrogen respectively.

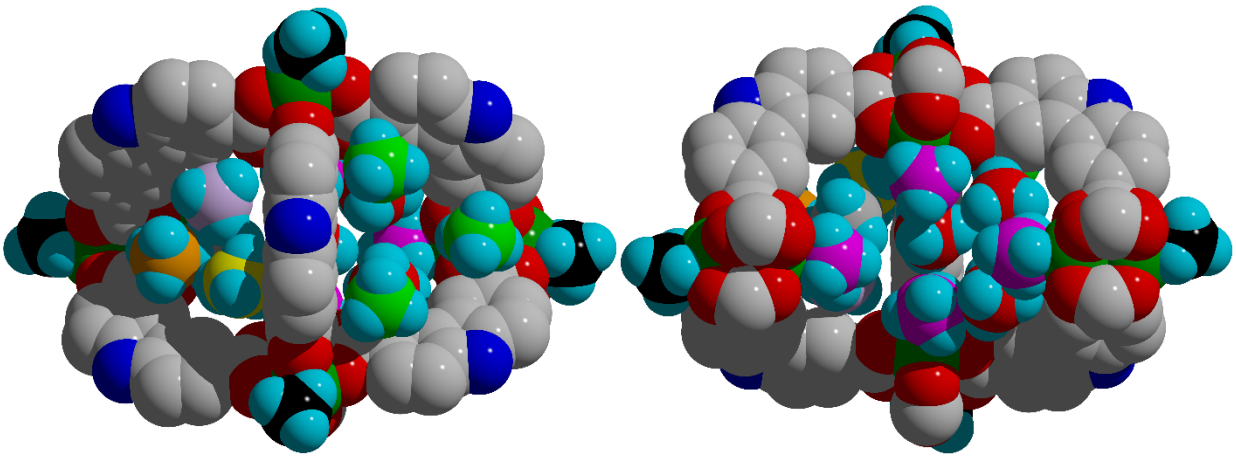

Figure S46. Space-filling representation of CD_4 adsorbed on the exterior (left) and interior (right) of the carbazole-based cage of PCN-81.

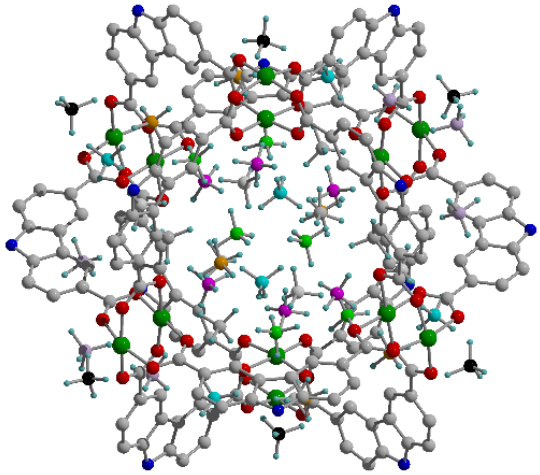

Figure S47. PCN-81 dosed with 3.71 equivalents of CD_4 per metal center solved via powder neutron diffraction with H-atoms omitted for clarity. Green, gray, red, and blue represent copper, carbon, oxygen, and nitrogen respectively.

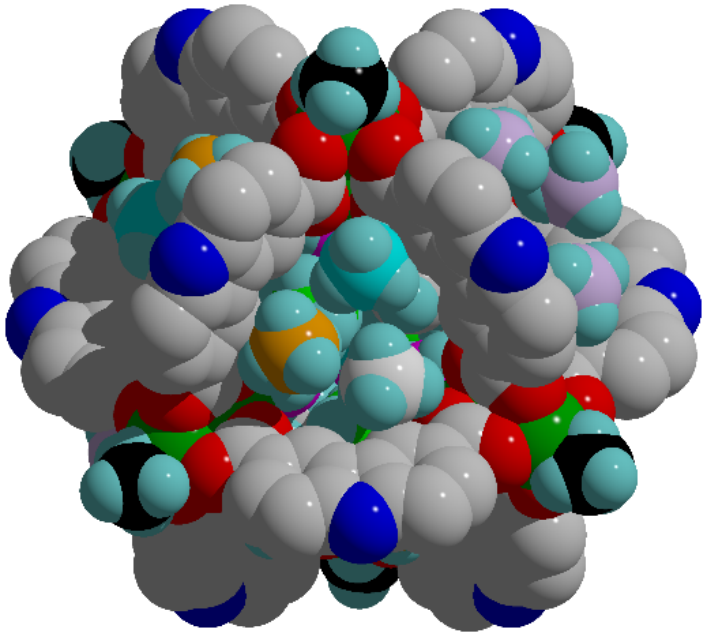

Figure S48. PCN-81 dosed with 3.71 equivalents of CD_4 per metal center solved via powder neutron diffraction shown in a space-filling model H-atoms omitted for clarity. Green, gray, red, and blue represent copper, carbon, oxygen, and nitrogen respectively.

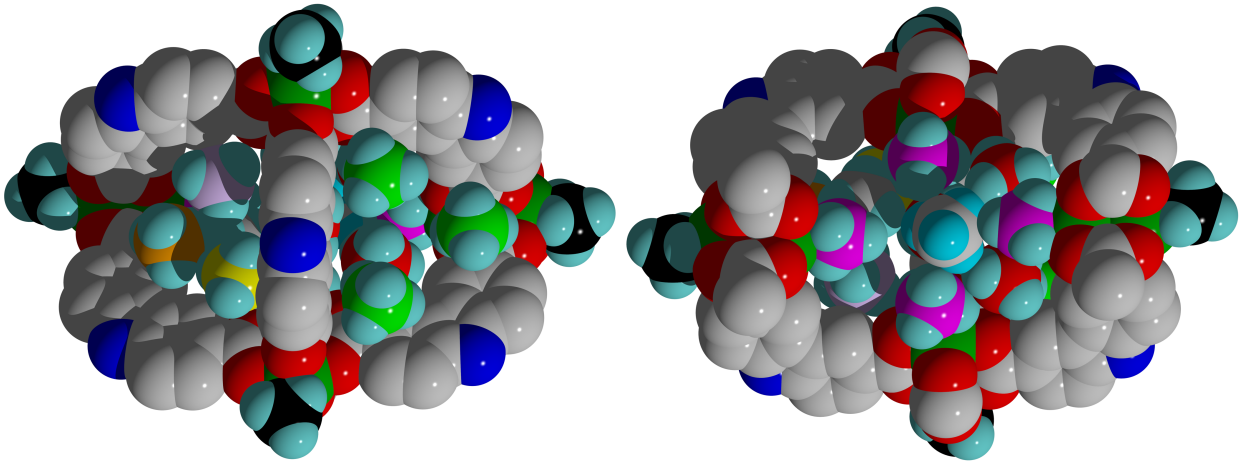

Figure S49. Space-filling representation of CD_4 adsorbed on the exterior (left) and interior (right) of the carbazole-based cage of PCN-81.

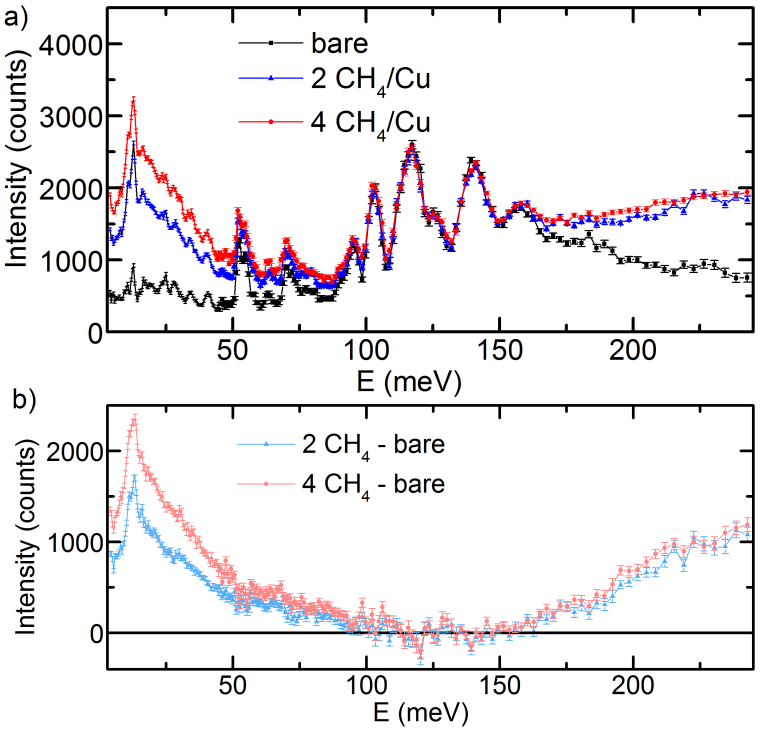

Figure S50. Inelastic Neutron Spectroscopy for PCN-81. a) Activated material (black squares) compared to 2 CH_4/Cu (blue triangles) and 4 CH_4/Cu (red circles). b) Difference curves for CH_4 loaded PCN-81.

References

1) Li, J.-R.; Timmons, D. J.; Zhou, H.-C. Interconversion between Molecular Polyhedra and Metal-Organic Frameworks. *J. Am. Chem. Soc.* **2009**, *131*, 6368-6369.
2) Arnaiz, F. J. A Convenient Way to Generate Hydrogen Chloride in the Freshman Lab. *J. Chem. Educ.* **1995**, *72* (12), 1139.
3) Lu, W.; Yuan, D.; Makal, T. A.; Wei, Z.; Li, J.-R.; Zhou, H.-C. Highly Porous Metal-Organic Framework Sustained with 12-Connected Nanoscopic Octahedra. *Dalton Trans.* **2013**, *42*, 1708-1714.
4) Levy, O.; Bogoslavsky, B.; Bino, A. Anhydrous Chromous Acetate Revisited – A Very Simple Synthetic Route. *Inorganica Chimica Acta.* **2012**, *391*, 179-181.
5) *Apex3*; Bruker AXS Inc.: Madison, WI, 2015.
6) Sheldrick, G. M. SHELXT – Integrated Space-Group and Crystal-Structure Determination. *Acta Cryst.* **2015**, *A71*, 3-8.
7) Sheldrick, G. M. Crystal Structure Refinement with SHELXL. *Acta Cryst.* **2015**, *C71*, 3-8.
8) Perry, Z.; Chen. Y.-P.; Bae, J.; Zhou, H.-C. Chromium (II) Metal-Organic Polyhedra as Highly Porous Materials. *ACS Appl. Mater. Interfaces.* **2017**, *9*, 28064-28068.
9) Spek, A. L. Structure Validation in Chemical Crystallography. *Acta Cryst.* **2009**, *D65*, 148-155.
10) Spek, A. L. PLATON SQUEEZE: A Tool for the Calculation of the Disordered Solvent Contribution to the Calculated Structure Factors. *Acta Cryst.* **2015**, *C71*, 9-18.
11) Udovic, T. J.; Brown, C. M.; Leão, J. B.; Brand, P. C.; Jiggets, R. D.; Zeitoun, R.; Pierce, T. A.; Peral, I.; Copley, J. R. D.; Huang, Q.; Neumann, D. A.; Fields, R. J. The Design of Bismuth-Based Auxiliary Filter for the Removal of Spurious Background Scattering Associated with Filter-Analyzer Neutron Spectrometers. *Nucl. Instruments Methods Phys. Res. Sect. A.* **2008**, *588*, 406-413.
12) Coelho, A. *Topas Academic v6*; Coelho Softw. (2017). http://www.topas-academic.net/.
13) Pawley, G. S. Unit-Cell Refinement from Powder Diffraction Scans. *J. Appl. Crystallogr.* **1981**, *14*, 357-361.
14) Andreev, Y. G.; MacGlashan, G. S.; Bruce, P. G. Ab initio Solution of a Complex Crystal Structure from Powder-Diffraction Data using Simulated-Annealing Method and a High Degree of Molecular Flexibility. *Phys. Rev. B.* **1997**, *55*, 12011-12017.
15) Rietveld, H. M. A Profile Refinement Method for Nuclear and Magnetic Structures. *J. Appl. Crystallogr.* **1969**, *2*, 65-71.
16) Hulvey, Z.; Vlaisavljevich, B.; Mason, J. A.; Tsivion, E.; Dougherty, T. P.; Bloch, E. D.; Head-Gordon, M.; Smit, B.; Long, J. R.; Brown, C. M. Critical Factors Driving the High Volumetric Uptake of Methane in Cu3(btc)2. *J. Am. Chem. Soc.* **2015**, *137*, 10816-10825.
17) Hamilton, W. C. Significance Tests on the Crystallographics R Factor. *Acta Cryst.* **1965**, *18*, 502-510.
18) Guo, Z.; Wu, H.; Srinivas, G.; Zhou, Y.; Xiang, S.; Chen, Z.; Yang, Y.; Zhou, W.; O'Keeffe, M.; Chen, B. A Metal-Organic Framework with Optimized Open Metal Sites and Pore Spaces for High Methane Storage at Room Temperature. *Angew. Chem. Int. Ed.* **2011**, *50*, 3178-3181.
19) Savage, M.; Da Silva, I.; Johnson, M.; Carter, J. H.; Newby, R.; Suyetin, M.; Besley, E.; Manuel, P.; Rudić, S.; Fitch, A. N.; Murray, C.; David, W. I. F.; Yang, S.; Schröder, M.

Observation of Binding and Rotation of Methane and Hydrogen within a Functional Metal-Organic Framework. *J. Am. Chem. Soc.* **2016**, *138*, 9119-9127.
20) Greathouse, J. A.; Cygan, R. T.; Simmons, B. A. Vibrational Spectra of Methane Clathrate Hydrates from Molecular Dynamics Simulation. *J. Phys. Chem. B.* **2006**, *110*, 6428-6431.
21) Ramya, K. R.; Pavan Kumar, G. V.; Venkatnathan, A. Raman Spectra of Vibrational and Librational Modes in Methane Clathrate Hydrates using Density Functional Theory. *J. Chem. Phys.* **2012**, *136,* 174305.